Circulation Research

ORIGINAL RESEARCH

Somatic Gain of KRAS Function in the Endothelium Is Sufficient to Cause Vascular Malformations That Require MEK but Not PI3K Signaling

Jason E. Fish,* Carlos Perfecto Flores Suarez*, Emilie Boudreau*, Alexander M. Herman, Manuel Cantu Gutierrez, Dakota Gustafson, Peter V. DiStefano, Meng Cui, Zhiqi Chen, Karen Berman De Ruiz, Taylor S. Schexnayder, Christopher S. Ward, Ivan Radovanovic, Joshua D. Wythe

RATIONALE: We previously identified somatic activating mutations in the *KRAS* (*Kirsten rat sarcoma viral oncogene homologue*) gene in the endothelium of the majority of human sporadic brain arteriovenous malformations; a disorder characterized by direct connections between arteries and veins. However, whether this genetic abnormality alone is sufficient for lesion formation, as well as how active KRAS signaling contributes to arteriovenous malformations, remains unknown.

OBJECTIVE: To establish the first in vivo models of somatic KRAS gain of function in the endothelium in both mice and zebrafish to directly observe the phenotypic consequences of constitutive KRAS activity at a cellular level in vivo, and to test potential therapeutic interventions for arteriovenous malformations.

METHODS AND RESULTS: Using both postnatal and adult mice, as well as embryonic zebrafish, we demonstrate that endothelial-specific gain of function mutations in *Kras* (G12D or G12V) are sufficient to induce brain arteriovenous malformations. Active KRAS signaling leads to altered endothelial cell morphogenesis and increased cell size, ectopic sprouting, expanded vessel lumen diameter, and direct connections between arteries and veins. Furthermore, we show that these lesions are not associated with altered endothelial growth dynamics or a lack of proper arteriovenous identity but instead seem to feature exuberant angiogenic signaling. Finally, we demonstrate that KRAS-dependent arteriovenous malformations in zebrafish are refractory to inhibition of the downstream effector PI3K but instead require active MEK (mitogen-activated protein kinase kinase 1) signaling.

CONCLUSIONS: We demonstrate that active KRAS expression in the endothelium is sufficient for brain arteriovenous malformations, even in the setting of uninjured adult vasculature. Furthermore, the finding that KRAS-dependent lesions are reversible in zebrafish suggests that MEK inhibition may represent a promising therapeutic treatment for arteriovenous malformation patients.

GRAPHICAL ABSTRACT: A graphical abstract is available for this article.

Key Words: brain ■ cell size ■ endothelium, vascular ■ models, animal ■ vascular disease

Editorial, see p 744 | In This Issue, see p 703 | Meet the First Author, see p 704

Brain arteriovenous malformations (bAVMs) are abnormal direct connections between arteries and veins that bypass a capillary network.[1] Because blood flow and pressure are not dissipated, the vein can become distended and enlarged. Over time, altered flow dynamics may lead to extensive remodeling of the conduit vessels into a tangled nidus; a hallmark of bAVMs.[2] Because of their propensity to leak or rupture, these

Correspondence to: Jason E. Fish, PhD, Toronto General Hospital Research Institute, University Health Network, Toronto Medical Discovery Tower, MaRS Bldg, 101 College St, 3-308, Toronto, ON M5G 1L7, Email jason.fish@utoronto.ca; or Joshua D. Wythe, PhD, Cardiovascular Research Institute, One Baylor Plaza, Baylor College of Medicine, Houston, TX 77030, Email joshua.wythe@bcm.edu

*J.E.F., C.P.F.S., and E.B. contributed equally to this article.

The Data Supplement is available with this article at https://www.ahajournals.org/doi/suppl/10.1161/CIRCRESAHA.119.316500.

For Sources of Funding and Disclosures, see page 741.

ORIGINAL RESEARCH

Novelty and Significance

What Is Known?

- Somatic mutations in the *KRAS* (*Kirsten rat sarcoma viral oncogene homologue*) gene are detected within the endothelial cells (ECs) lining the vessels of brain arteriovenous malformations (bAVMs) in the majority of patients with sporadic lesions.
- Histological analysis shows that these activating mutations in KRAS lead to the constitutive activation of the downstream MAPK/MEK (mitogen-activated protein kinase kinase 1)/ERK (extracellular signal-regulated kinase) signaling pathway.
- In cultured ECs, expression of active KRAS increases migration and alters cell shape and actin dynamics without affecting proliferation.

What New Information Does This Article Contribute?

- In both mouse and zebrafish models, expression of mutant KRAS in the endothelium is sufficient to induce bAVMs in vivo.
- In vivo, ECs expressing active KRAS have increased cell size and increased sprouting behavior, and vessels are tortuous with dilated lumens, and abnormal connections occur between arteries and veins. Critically, these ECs do not show increased proliferation.
- Inhibition of MEK/ERK signaling, but not PI3K activity can suppress the KRAS-induced gene signature in cultured ECs, and can rescue lesion formation and reverse established arteriovenous shunts.

Arteriovenous malformations are the leading cause of brain hemorrhage in children and young adults. Most bAVMs are sporadic (ie, no familial history of inheritance). We recently showed that somatic activating *KRAS* mutations occur in the endothelium of the majority of these lesions, and that this leads to activation of the MAPK/MEK/ERK signaling pathway in cultured ECs. This suggested that pharmacological treatments for brain arteriovenous malformations may be possible. However, whether somatic *KRAS* mutations actually cause these vascular lesions, and the requirement of the MAPK/MEK/ERK pathway in maintaining these malformations, were not known. Furthermore, the mechanisms that lead to sporadic arteriovenous malformation have not been deciphered. Here, we establish the first animal models of KRAS-dependent bAVMs in both mice and zebrafish. We demonstrate that expression of active KRAS in the endothelium of the brain is sufficient to produce bAVMs. At the cellular level, blood vessels expressing active KRAS have expanded lumens, ectopic sprouting, and abnormal connections between arteries and veins. At the molecular level, we identify MEK-dependent angiogenic gene networks that are activated in KRAS-expressing ECs. Importantly, inhibition of MEK in our zebrafish model reveals that established arteriovenous shunts can be reversed, giving hope that such approaches may be useful in a clinical setting.

Nonstandard Abbreviations and Acronyms

AVM	arteriovenous malformation
bAVM	brain arteriovenous malformation
DA	dorsal aorta
EC	endothelial cell
ISV	intersomitic vessel

vascular malformations are the leading cause of hemorrhagic stroke in children and young adults.[1] Current therapy is limited to surgical resection, endovascular embolization or stereotactic radiosurgery, but this carries significant risk and is not always possible depending on location. No pharmacological interventions have been developed, which is due to our rudimentary understanding of the biology underlying the origin and progression of sporadic bAVMs. By performing exome sequencing on resected patient bAVM tissues and matching peripheral blood as a germline control, our group found that somatic activating mutations in the gene *KRAS* (*Kirsten rat sarcoma viral oncogene homologue*)—which encodes RAS GTPase (guanosine triphosphate hydrolase)—occurred in the endothelium of ≈60% of all sporadic bAVMs.[3] This finding of somatic *KRAS* mutations has since been confirmed by others.[4–7] However, no preclinical studies have been performed to test whether active *KRAS* mutations are sufficient to drive the formation of arteriovenous malformations (AVMs).

KRAS activating mutations have been observed in both codon 12 (G12V, G12D, G12C) and in codon 61 (Q61H).[3–7] These same mutations are highly prevalent in cancer, where they constitutively activate KRAS by preventing GTP hydrolysis.[8] Activating mutations have also been identified in *BRAF* and *MAP2K1/MEK* (*mitogen-activated protein kinase kinase* 1) in AVMs.[6,7] Each of these mutated genes function in the MEK/ERK (extracellular signal-regulated kinase) kinase cascade, suggesting this pathway plays a key role in AVM pathogenesis. Indeed, we observed robust MEK/ERK activity in all bAVM tissues that we examined, even those that did not contain

detectable *KRAS* mutations, indicating that excessive activity of this pathway is a central feature in the pathogenesis of these lesions.[3]

Interestingly, somatic mutations in the endothelium have been observed in several other vascular malformations, including capillary malformations and venous malformations, but the mutations and signaling pathways in these diseases are distinct.[9–13] Based on this information, targeted therapies for venous malformations have been tested in slow-flow lesions in patients, with some success.[14–16] MEK signaling has been implicated in artery development[17–19] and angiogenesis,[20,21] and we previously showed that inhibition of the MEK pathway could suppress abnormal endothelial cell (EC) gene expression networks and morphology in active KRAS-transfected cells in vitro.[3] These findings suggest that exploration of MEK/ERK pathway inhibition may be warranted in sporadic bAVM patients. This is intriguing given the recent approval of several MEK inhibitors for treating cancer.[22] However, the failure to demonstrate that KRAS activation definitively leads to bAVMs in animal models remains a significant hurdle to testing these, and other novel therapies in a preclinical setting.

Thus, we set out to create mouse and zebrafish models of KRAS-induced, sporadic bAVMs. We found that pan-endothelial expression of constitutively active KRAS led to early postnatal lethality in mice, with focal cranial hemorrhage. However, both central nervous system-specific postnatal endothelial gain of KRAS activity, as well as later pan-endothelial induction in adults, bypassed this early lethality and led to dilated vessels and bAVMs. Similar phenotypes were observed upon endothelial-specific expression of mutant KRAS in the developing zebrafish, as embryos demonstrated overt hemorrhage and clear AV shunts, with accompanying alterations in vascular morphogenesis, including increased EC size, ectopic sprouting, and expanded vascular lumens. Notably, brain hemorrhage and existing AV shunts were partially rescued by pharmacological inhibition of MEK activity. Collectively, these results establish novel animal models for the future study of *KRAS*-mediated bAVM progression. Furthermore, this study indicates that MEK inhibition is a promising therapeutic strategy for treating bAVMs in humans.

METHODS

The authors declare that all supporting data are available within the article and its Data Supplement. RNA-seq data has been deposited at the Gene Expression Omnibus, our informatics RStudio pipeline is contained within the Data Supplement, and all plasmids will be deposited at Addgene. Reasonable requests for fish or mice will be fulfilled by the corresponding authors.

A complete description of Methods is included in the Data Supplement. Please see the Major Resources Table in the Data Supplement.

RESULTS

Early Postnatal Expression of KRAS^{G12D} in the Murine Endothelium Results in Cerebral Hemorrhage and Death

To explore the cellular and molecular mechanisms that underlie bAVMs in patients harboring somatic *KRAS* gain of function mutations, we generated compound transgenic mice that harbor a tamoxifen-inducible, EC-specific Cre recombinase (*Cdh5(PAC)-CreERT2,* which we will refer to hereafter as *Cdh5-CreER*)[23] and a conditional, Cre-activatable mutant *Kras* allele.[24] In this lox-stop-lox mutant *Kras* conditional mouse strain (referred to as *Kras^{G12D}*), expression of the constitutively active *Kras^{G12D}* mutant transcript requires Cre-dependent removal of a transcriptional stop cassette (Online Figure IA). This conditional mutant allele is targeted to the endogenous *Kras* locus, which ensures that physiological levels of constitutively active *Kras^{G12D}* transcript are only expressed from the native promoter following removal of the stop cassette. Of note, activation of the *Cdh5-CreER* driver at P1 led to uniform expression of a recombined *Rosa26^{RFP}* lineage reporter throughout the entire brain vasculature at P14 (Online Figure II). Kaplan-Meier survival analysis determined that administration of tamoxifen at P1 to *Cdh5-CreER; Kras^{G12D}* (hereafter referred to as inducible EC-specific *Kras^{G12D}*, or *iEC-Kras^{G12D}*) mice on a variety of fluorescent reporter backgrounds (see Methods in the Data Supplement) resulted in significant lethality beginning around P12 (Online Figure IA and IB; Control, n=48; *iEC-Kras^{G12D}*, n=138). Gross morphological analyses of surviving animals at P21 revealed an incompletely penetrant phenotype of focal intracranial hemorrhage (Control, n=0/116; *iEC-Kras^{G12D}*, n=11/32), which was confirmed via 3D imaging of the cortical cerebrovasculature via light sheet microscopy (Online Figure IC through IF). However, cortical AVMs were not observed. In contrast to other established models of bAVMs, such as Notch gain of function,[25] the cerebral vessels did not appear dilated, but instead appeared thin and fragile (Online Figure IF; Online Movies I and II). Vessel density within the brain at P21 was indistinguishable between *Kras* mutants (n=5) and control animals (n=7; Online Figure III), suggesting that KRAS gain of function may not stimulate EC proliferation, in agreement with our previous in vitro studies.[3] Analysis of *iEC-Kras^{G12D}* mice on a pure *Rosa26^{RFP}* reporter background recapitulated the early postnatal lethality, but mutants failed to show frequent cranial hemorrhage (n=1/6) or cortical bAVMs (n=0/6) at P14 (Online Figure IVA through IVD). The lethality of *iEC-Kras^{G12D}* pups was not due to a failure to thrive, as they were of comparable size and weight to their littermate controls (Online Figure IVG and IVH). Analysis of visceral organs likewise did not reveal obvious hemorrhage in the intestines, lung, or liver at P14

(Online Figure IVE and IVF). Assessment of cardiac structure and function at P14 and P21 failed to reveal any consistent alterations in *iEC-Kras^{G12D}* mice (Online Figure V). As we only analyzed surviving animals at P14 and P21, and these animals did not feature either bAVMs or organ hemorrhage, and showed mostly normal cardiac performance, the cause of this early postnatal lethality remains unclear. Nevertheless, these results led us to posit that more time and perhaps hemodynamic feedback are required to form bAVMs, and that early lethality in this model precludes lesion formation.

Postnatal Expression of KRAS^{G12D} in the Murine Central Nervous System Endothelium Bypasses Early Lethality and Produces bAVMs

To more specifically assess the role of elevated KRAS activity in the cerebrovasculature, we utilized the *Slc1o1c1(BAC)-CreER*[26] driver line to restrict mutant KRAS expression to the brain endothelium. This approach has the added benefit of more closely mimicking the location of somatic gain of *KRAS* function mutations observed in human patients.[3] Females harboring a Cre-dependent *Rosa26^{RFP}* reporter were crossed to males containing the *Slc1o1c1-CreER* allele. RFP signal (a visual readout for CreER activity) was observed in the endothelium of the brain and retina, likely reflecting a general central nervous system-wide endothelial activity of the transgene (Online Figure VIA). In contrast to previous reports using the same reporter,[26] we observed CreER activity in the absence of tamoxifen (Online Figure VIB and VIC). With this leakiness in mind, we maintained the *Kras^{G12D}* allele in *Rosa26$^{RFP/RFP}$* dams, separate from *Kras$^{WT/WT}$*; *Slc1o1c1-CreER* driver sires, then treated all offspring with tamoxifen at P1. Notably, immunohistochemical analysis of 8-week-old brains revealed robust and uniform labeling of the cerebrovasculature throughout the brain, as well as expression in nonvascular tissues, as previously described[26] (Online Figure VII).

Initiation of mutant *Kras^{G12D}* expression using the inducible brain EC driver *Slco1c1-CreER* (hereafter referred to as *ibEC-Kras^{G12D}*) at P1 did not affect survival up to 8 weeks of age (Control, n=0/47 dead; *ibEC-Kras^{G12D}*, n=0/28 dead; Figure 1A and 1B). Unlike the *iEC-Kras^{G12D}* pups at P21, *ibEC-Kras^{G12D}* brains lacked overt signs of hemorrhage at P21 (Control n=0/14; *ibEC-Kras^{G12D}* n=0/7; Figure 1C). This was also the case in 8-week-old adult animals, where we only rarely observed intracranial hemorrhage in the *Kras* mutants compared with their control littermates (Control, n=0/47; *ibEC-Kras^{G12D}*, n=1/28; Figure 1D and 1E). Notably, perfusion with fluorescent-labeled lectin, followed by epifluorescence examination, revealed the presence of bAVMs in *ibEC-Kras^{G12D}* adults at 8 weeks of age (n=11/21; Figure 1F and 1G). These abnormalities, which occurred in the cortex, just anterior to the cerebellum, as well as near the olfactory bulb, were not detected in control animals at 8 weeks of age (n=0/32; Figure 1F and 1G). Optical clearing and light sheet confocal microscopy revealed that the vasculature surrounding these bAVMs was abnormal, as the vessels appeared tortuous and dilated, similar to the niduses associated with these lesions in human patients, whereas these vessels appeared normal in control animals (Figure 1F, far right, upper and lower panels; also see Online Movies III and IV).

Pan-Endothelial Expression of KRAS^{G12D} in Adult Mice Bypasses Lethality and Produces bAVMs

We next sought to determine whether *Kras* gain of function throughout the adult murine endothelium was sufficient to produce bAVMs. Interestingly, in endothelial-specific loss of function mouse models of Hereditary Hemorrhagic Telangiectasia, such as endothelial-specific loss of *Alk1* or *Eng*, central nervous system AVMs arise if loss of function is induced in early embryonic stages[27–30]; however, they only appear in adult stages with the addition of an exogenous angiogenic stimulus.[28,31] Similarly, gain of constitutive Notch1 or 4 activity must be initiated during the early postnatal period to produce bAVMs.[29] Treatment of *iEC-Kras^{G12D}* and control littermates with tamoxifen between 2 and 4 months of age did not affect overall survival up to 8 weeks later (Control, n=0/23; *iEC-Kras^{G12D}*, n=0/19; Figure 2A and 2B). In a pilot cohort, no differences in viability were detected up to 36 weeks later (Control, n=0/4; *iEC-Kras^{G12D}*, n=0/3; Figure 2A and 2B). In contrast to our early postnatal experiments, pan-endothelial induction of mutant KRAS expression in adult mice failed to induce hemorrhage after 8 weeks (Control, n=0/23; *iEC-Kras^{G12D}*, n=0/19; Figure 2C and 2D). However, this induction regime was sufficient to induce bAVMs in *iEC-Kras^{G12D}* animals within 8 weeks of treatment in more than half of all animals examined (Control, n=0/15; *iEC-Kras^{G12D}*, n=6/11; Figure 2E and 2F). A similar phenotypic penetrance was observed 36 weeks after induction in a small cohort with a limited sample size (Control, n=0/4; *iEC-Kras^{G12D}*, n=2/3; Figure 2G). Thus, expression of *Kras^{G12D}* in the endothelium is sufficient to induce bAVMs in both postnatal and adult mice.

Expression of Mutant KRAS in the Endothelium of Embryonic Zebrafish Alters Vascular Morphology

To assess the consequences of expressing active KRAS in the endothelium at a cellular level, we utilized embryonic zebrafish. Tol2-transposable element-flanked transgenes, with expression of either fluorescently-tagged wild-type (WT) or mutant human KRAS under the control of an endothelial-specific *kdrl* promoter, were injected

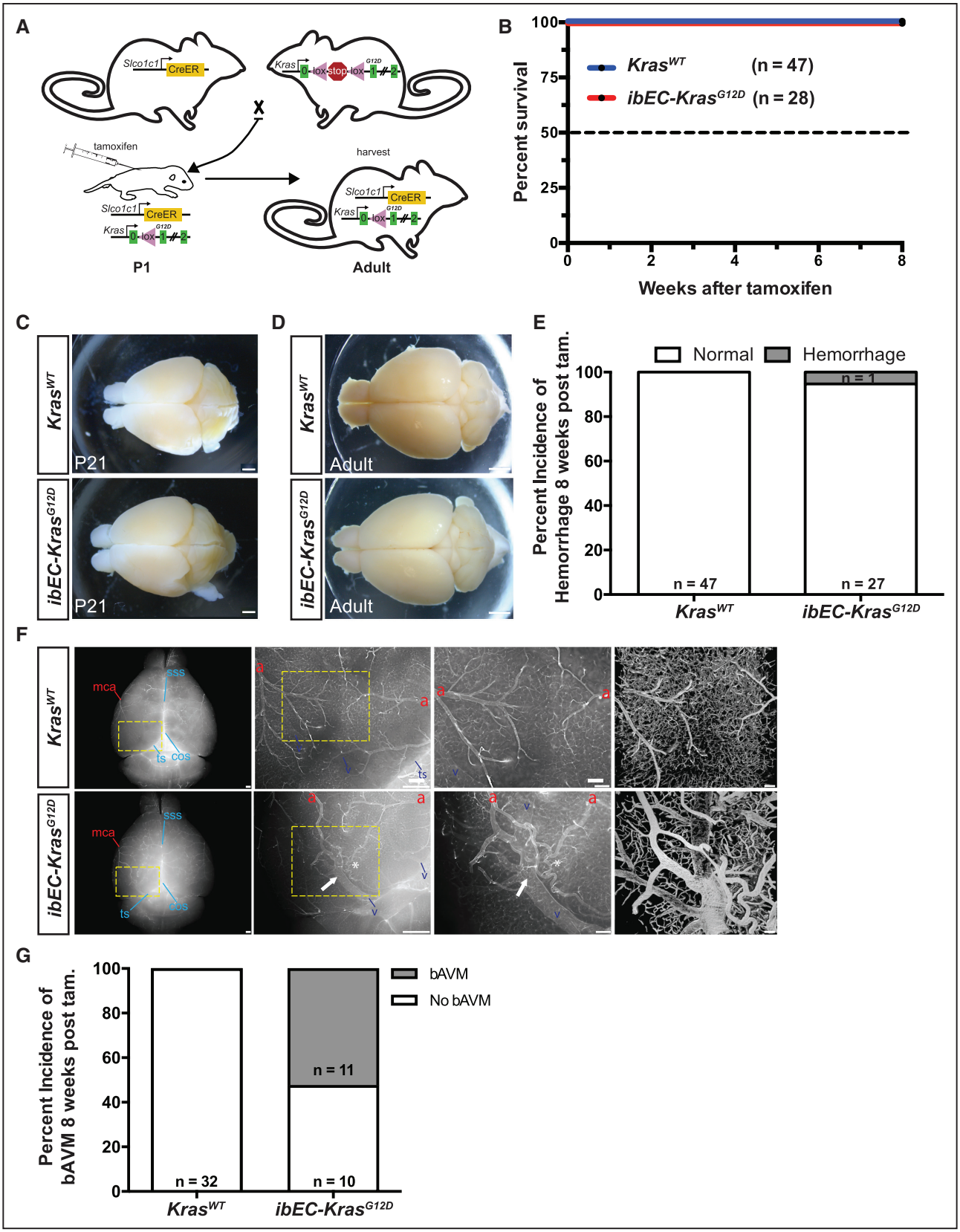

Figure 1. Postnatal expression of active KRAS (Kirsten rat sarcoma viral oncogene homologue) in the murine central nervous system endothelium bypasses early lethality and produces brain arteriovenous malformations.
A, Breeding scheme for generating inducible brain endothelial cell KRAS mutant mice (*ibEC-Kras*^{G12D}). Tamoxifen is delivered to pups at P1 and tissues are harvested at 8 wk of age. **B**, No survival defects were observed in *ibEC-Kras*^{G12D} mice or control *Kras*^{WT} littermates. (*Continued*)

along with transposase mRNA at the 1 to 4 cell stage to generate mosaic embryos (Figure 3A). Importantly, the mosaic nature of *KRAS* expression in this transient transgenic system mimics the somatic nature of *KRAS* mutations in human patients. Expression of N-terminal EYFP-tagged human KRAS^{WT} in the endothelium did not have an appreciable effect on the phenotype of ECs in the intersomitic vessels (ISVs) or in the dorsal aorta (DA) (Figure 3B). In contrast, expression of N-terminal EGFP-tagged human KRAS^{G12V} dramatically altered EC morphology (Figure 3C through 3E). Ectopic sprouting defects were apparent in 39.0±6.7% of ISVs imaged at 48 hpf that contained KRAS^{G12V}-expressing ECs (Figure 3C[i and ii]; arrows and Figure 3F). At earlier stages (ie, 36 hpf), ectopic sprouts containing numerous filopodia could be visualized in *Tg*(*kdrl*:LifeAct-GFP) embryos injected with *kdrl:*mScarlet-KRAS^{G12V} (Figure 3D). Additionally, 54.1±7.0% of ISVs expressing KRAS^{G12V} had a noticeably larger diameter, and of these ≈86% had lamellipodia-like protrusions that resulted in misshapen, bulbous vessels (Figure 3C[ii and iii]; arrowheads, Figure 3E, Figure 3G). The lumen of KRAS^{G12V}-expressing ISVs was expanded, as evidenced by an abundance of *gata1*:dsRed-expressing red blood cells within the ISV lumen (Figure 3E). Abnormal morphology was also noted when KRAS^{G12V}-expressing cells were located in the DA or posterior cardinal vein (Figure 3C[i and ii]; arrowheads). Similar phenotypes were evident in ISVs expressing BFP-tagged KRAS^{G12D} in the endothelium (Online Figure VIIIA and VIIIB). The ectopic sprouting and expanded vessel diameter phenotypes were confined to ISVs containing mutant KRAS-expressing ECs, as transgene-negative ISVs were phenotypically normal (Figure 3F and 3G). However, ectopic sprouts were observed occasionally in nontransgenic ECs adjacent to mutant KRAS-expressing cells (Online Figure VIIIA), suggestive of noncell autonomous effects.

We next determined whether EC hypertrophy (eg, enhanced cell size) or hyperplasia (eg, increased cell number) were responsible for the wider ISVs. Individual ECs expressing active KRAS had highly abnormal cellular shapes (Figure 4A) and KRAS^{G12V}-expressing ISVs had significantly (≈2.1-fold) increased ISV diameters (Figure 4B) and expanded blood volumes (Figures 3E and 4A). Of note, the effect on ISV diameter was cell autonomous as regions of ISVs that lacked transgene expression were of normal diameter (Figure 4A). Quantification of the number of ECs per ISV revealed that ISV dilation was not likely due to an augmented number of cells, as there was only a modest, nonsignificant (≈1.17-fold) increase in the number of ECs (Figure 4C), but the average size of ECs was significantly increased by ≈1.7-fold (Figure 4D). To further assess the ability of active KRAS signaling to alter cell size, we quantified cell area in human umbilical vein ECs electroporated with control or KRAS^{G12V} constructs. This revealed a ≈1.9-fold increase in cell size in cells expressing mutant KRAS (Figure 4E and 4F), consistent with our previous observations.[3]

Activated KRAS Expression Leads to Arteriovenous Shunting and is Associated With Cranial Hemorrhages

Observing blood flow by bright field microscopy or visualizing fluorescently labeled red blood cells in *Tg*(*gata1:*dsRed) embryos revealed that KRAS^{G12V} expression in the endothelium resulted in AV shunts between the DA and the CV (Figure 5A and 5B). Quantification revealed that 47±4.5% of embryos injected with *kdrl:EGFP-KRAS^{G12V}* developed shunts in the distal axial vasculature at 48 hpf (Figure 5C). In contrast, embryos injected with *kdrl:EYFP-KRAS^{WT}* did not have a significant increase in the number of shunts (Figure 5C; Online Figure VIIIC). AV shunts were also prevalent in *Tg* (*kdrl:*LifeAct-GFP) embryos expressing BFP-KRAS^{G12D} under the control of *kdrl* regulatory elements, and this was accompanied by a breakdown of the normal separation between the DA and posterior cardinal vein, and a disruption of actin polymerization (Figure 5D).

Endothelial-specific expression of KRAS^{G12V} in zebrafish was associated with cranial hemorrhages in 19.7±4.6% of embryos, as visualized by cranial blood pooling by bright field imaging (not shown) or confocal microscopy in *Tg*(*gata1*:dsRed) embryos (Figure 5E and 5F). In contrast, expression of KRAS^{WT} did not induce this phenotype (Figure 5F; Online Figure VIIIC). Examination of vascular morphology revealed that KRAS^{G12V} expression led to a malformed cerebral vasculature,

Figure 1 Continued. C, Representative phase microscopy images of the dorsal surface of the brain at P21 show no cerebral hemorrhages in either *ibEC-Kras^{G12D}* mice (n=0/7) or control littermates (n=0/14; quantification not shown). Scale bar=500 µm. **D**, Representative phase microscopy images of the dorsal surface of the brain at 8 wks. Scale bar=500 µm. **E**, Quantification of the incidence of hemorrhage at 8 wk of age in both control (n=0/35) and *ibEC-Kras^{G12D}* mice (n=1/19). Fisher exact test; *P*=0.373. **F**, Representative dorsal surface view, olfactory bulb at the top and cerebellum at the bottom, via direct fluorescence microscopy of an 8-week-old adult mouse brain following perfusion with fluorescent lectin. Arteriovenous shunts, or fusions, between cerebral arteries (red letter a) and veins (blue letter v), as well as venous dilation (white arrow) and tortuosity (asterisk) are evident in *ibEC-Kras^{G12D}* animals but not the control littermates at 8 wk of age. Magnified areas (yellow boxes) are shown in the panels to the right. Far right panels are flattened reconstructions of volume rendered images of the cortical vasculature following CLARITY clearing and lightsheet confocal microscopy. Scale bar=500 µm for first 2 (left to right) upper and lower panels for wild-type and mutant brain images (with yellow dashed boxes), and = 100 µm for upper and lower far right magnified images. **G**, Quantification of the incidence of brain arteriovenous malformation (bAVM) at 8 wk of age. Fisher exact test; $P=4.6\times10^{-6}$. COS indicates confluence of sinus veins; MCA, middle cerebral artery; SSS, superior sagittal sinus vein; and TS, transverse sinus vein.

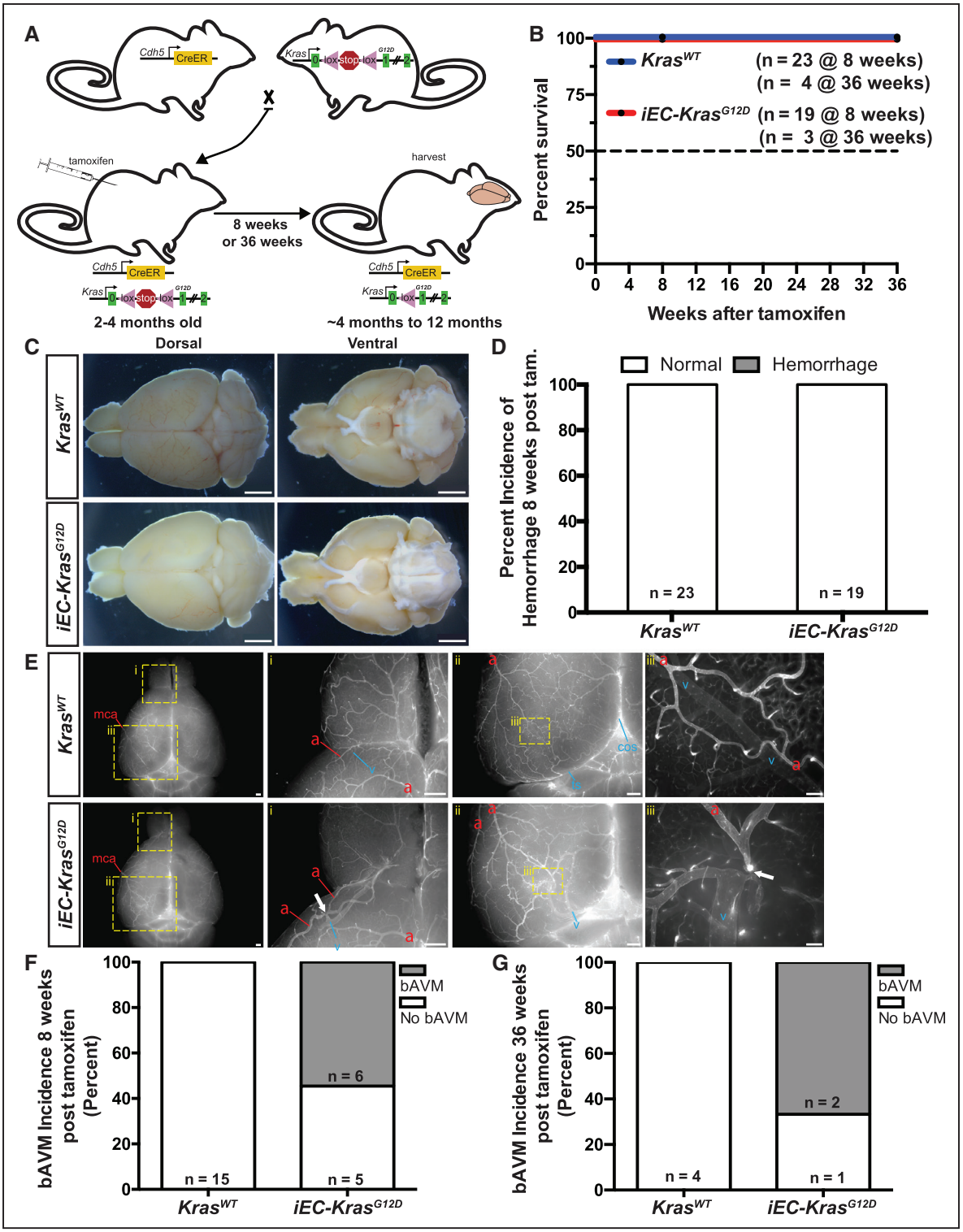

Figure 2. Pan-endothelial expression of active KRAS (Kirsten rat sarcoma viral oncogene homologue) in adult mice induces brain arteriovenous malformations.

A, Representative model for induction of pan-endothelial mutant KRAS activity in adult mice. **B**, No survival defects were observed in KRAS mutant mice or control animals up to 8 and 36 wk following induction. **C**, No evidence of hemorrhage was detected at 8 wk post-treatment in adult KRAS mutant or control animal brains. Representative phase microscopy images of the dorsal and ventral surfaces of the brain are shown. Scale bar=500 μm. **D**, Quantification of the incidence of cranial hemorrhage 8 wk after initiating tamoxifen treatment at 2 to 4 mo of age. **E**, Representative whole mount epifluorescent views following perfusion of fluorescent-conjugated tomato lectin reveal the presence of brain arteriovenous malformations (bAVMs; white arrow) just distal to the olfactory bulb (**i**) and in the cortex just proximal to the cerebellum (**Eii** and **Eiii**). a=artery, v=vein. Scale bar=500 μm for far-left panels, and **Ei** and **Eii**, and scale bar=100 μm for **Eiii**. **F**, Quantification of bAVM incidence 8 wk post tamoxifen induction. Fisher exact test; *P*=0.002. **G**, Quantification of the incidence of bAVM at 36 wk post–tamoxifen induction. The sample size was too small for statistical analysis.

ORIGINAL RESEARCH

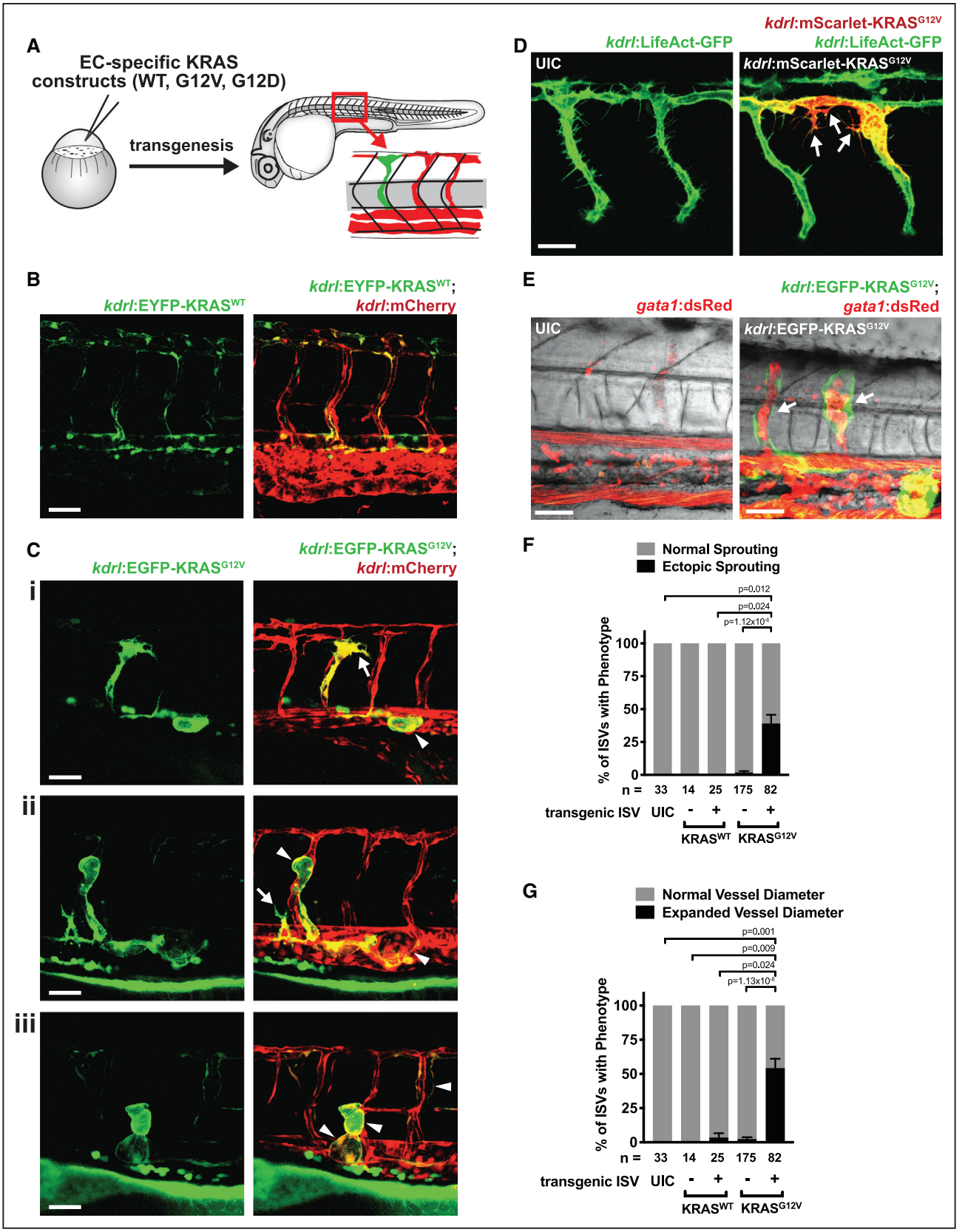

Figure 3. Expression of active KRAS (Kirsten rat sarcoma viral oncogene homologue) in the endothelium of embryonic zebrafish alters cellular morphology.

A, Schematic of mosaic analysis of KRAS expression in the endothelium. Wild-type KRAS (KRAS^{WT}) or mutant KRAS (KRAS^{G12V} or KRAS^{G12D}) were expressed under the control of an endothelial-specific promoter, *kdrl*. **B**, Representative image of a *Tg*(*kdrl*:mCherry) embryo injected with a *kdrl*:EYFP-KRAS^{WT} construct. No changes in cellular phenotype were noted. 52 h post-fertilization (hpf). (*Continued*)

including larger diameter vessels and abnormal connections between vessels (Figure 5G).

KRAS Signaling Does Not Alter AV Identity, but Activates Angiogenic Signaling

To determine whether expression of mutant KRAS affected AV identity, we examined the activity of fluorescent arterial reporters in vivo. The *Tg*(*Dll4*:GFP) reporter line has high activity in arterial ISVs and the DA of the developing embryo. We did not observe an increase in the already robust reporter activity in ISVs or the DA in embryos expressing $KRAS^{G12D}$ in the endothelium (Online Figure IXA). However, we found that *Dll4* reporter activity was elevated in shunts between the DA and posterior cardinal vein and expression was observed in some $KRAS^{G12D}$-expressing venous cells (Online Figure IXA). However, when we examined Notch activity—a critical determinant of AV identity—using the transgenic Notch reporter line *Tg*(*Tp1:*GFP), only modest levels of Notch signaling were evident in shunts and no expression was detected in $KRAS^{G12V}$-expressing venous cells (Online Figure IXB). This suggests that expression of active KRAS may not dramatically alter AV identity. As we previously demonstrated that the *Dll4*:GFP reporter is regulated by VEGF signaling and requires a single, intact ETS transcription factor DNA binding sequence, and is largely Notch-independent, we assessed whether ETS reporter activity was altered by KRAS expression. To do so, we generated a novel ETS reporter line by concatemerizing the ETS B-site of the murine *Dll4* intron 3 enhancer (8X).[19] Reporter activity was detected in ECs of some of the sprouting ISVs and the DA at 24 hpf. At later developmental stages (ie, 48 and 72 hpf), low levels of reporter activity remained confined to the DA and select ISVs (Online Figure IXC). ETS reporter activity was induced in $KRAS^{G12V}$-expressing cells, including within shunts and in venous cells, and was also elevated in neighboring, transgene-negative cells (Online Figure IXD).

Activated KRAS Enhances EC Permeability In Vitro in a MEK-Dependent Manner

Our previous study revealed that KRAS-driven downregulation of VE-Cadherin at cell-cell junctions in cultured ECs required MEK activity.[3] To further explore the role of KRAS in EC permeability and integrity, we performed a transwell leak assay in cultured human umbilical vein ECs. $KRAS^{G12V}$ expression enhanced EC permeability by ≈2-fold compared with ECs electroporated with a control plasmid (Figure 6A). Importantly, permeability was reduced by treatment of $KRAS^{G12V}$-expressing cells with 2 different MEK inhibitors, SL327 or U0126, for 18 hours before the addition of the FITC tracer, but was not affected by addition of the PI3K inhibitor (PI3Ki), LY294002 (Figure 6A), despite significant inhibition of pAKT levels (Online Figure XA). To further determine the requirement for PI3K and MEK kinase activity downstream of precocious KRAS activation in ECs, we performed transcriptional profiling in human umbilical vein ECs electroporated with empty vector or $KRAS^{G12V}$, followed by treatment with LY294002, U0126 or vehicle control. In total, $KRAS^{G12V}$ expression upregulated 460 genes and downregulated 236 genes (log_2-fold change >0.5 or <—0.5 and adjusted *P*-value <0.1; Figure 6B). Gene ontology analysis showed that $KRAS^{G12V}$ expression upregulated processes such as angiogenesis, cell cycle, regulation of MAP kinase activity, and RNA processing, among others (Figure 6B and 6C). Conversely, $KRAS^{G12V}$ expression led to downregulation of such processes as cytokine production, response to stress, and immune responses (Figure 6B and 6C). Further analysis of KRAS-expressing cells treated with PI3K inhibitors or MEK inhibitors identified 147 KRAS-induced, MEK-dependent targets that fell into such categories as blood vessel development, regulation of cell migration, and RNA processing (Figure 6D and 6E). Critically, KRAS-induced processes that required MEK activity—such as angiogenesis and cell migration—were not affected by PI3Ki (Figure 6F and 6G). Remarkably, PI3Ki only downregulated 21 unique targets, with just a single GO term emerging (Figure 6E). Additional analyses of this dataset can be found in Online Figures XI through XIII. Collectively, these results demonstrate that a subset of specific phenotypic and molecular changes induced by $KRAS^{G12V}$ expression in ECs require MEK, but not PI3K.

Inhibition of MEK Activity, but Not PI3K Signaling, Rescues Vascular Defects in $KRAS^{G12D}$-Expressing Embryos

To assess the importance of the MEK signaling pathway for shunt formation, embryos were treated with 1 μM of

Figure 3 Continued. C, Representative images of *Tg*(*kdrl*:mCherry) embryos injected with a *kdrl*:EGFP-$KRAS^{G12V}$ construct. Arrows indicate ectopic sprouting, while arrowheads indicate vessels with enlarged vessel diameter. **Ci**; 48 hpf, **Cii** and **Ciii**; 52 hpf. **D**, Representative images of *Tg*(*kdrl*:LifeAct-GFP) embryos injected with a *kdrl*:EGFP-$KRAS^{G12V}$ construct or an uninjected control (UIC). Arrows indicate ectopic sprouts. 36 hpf. **E**, Representative image of a *Tg*(*gata1*:dsRed) embryo injected with a *kdrl*:EGFP-$KRAS^{G12V}$ construct or an UIC. Arrows indicate expanded, blood-filled lumens in intersomitic vessels (ISVs) expressing $KRAS^{G12V}$. 64 hpf. Quantification of ectopic sprouting (**F**) or expanded vessel diameter (**G**) phenotypes in ISVs containing cells expressing the *kdrl*:$KRAS^{WT}$ or *kdrl*:$KRAS^{G12V}$ transgene (+) or in transgene-negative (—) ISVs or in ISVs in UIC embryos at 48 hpf. Shown is the mean±SEM of the percentage of embryos with the indicated phenotype across multiple experiments. The total number of ISVs assessed is shown below. Kruskal-Wallis test with Dunn multiple comparisons test. Scale bar=50 μm for **B**, **C**; 30 μm for **D**, **E**.

ORIGINAL RESEARCH

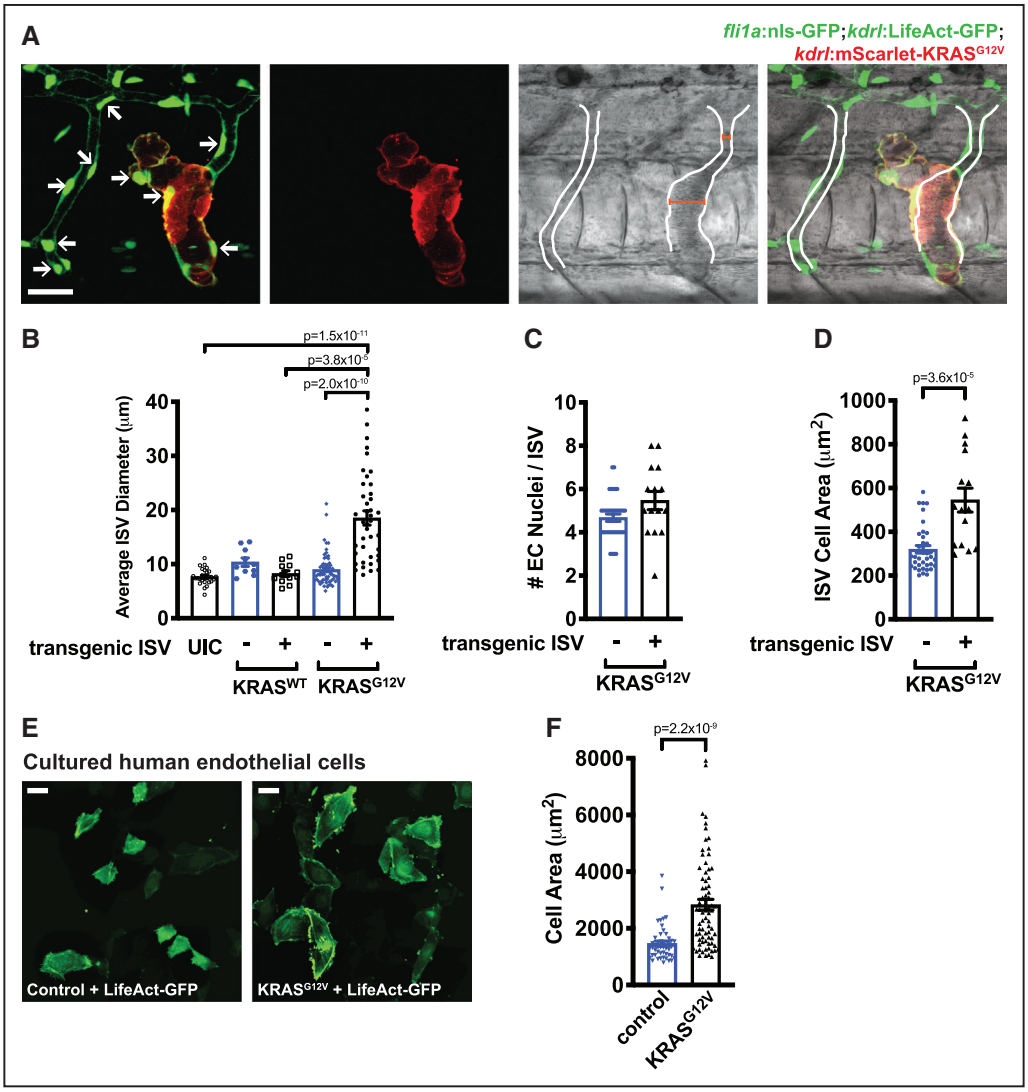

Figure 4. Active KRAS (Kirsten rat sarcoma viral oncogene homologue) expression increases the size of endothelial cells and expands vessel diameter.

A, Representative composite brightfield/fluorescent images of a *Tg* (*fli1*:nls-GFP; *kdrl*:LifeActGFP) embryo injected with *kdrl*:Scarlet-KRAS^{G12V} showing altered vessel morphology and expanded lumen (outlined from brightfield image of blood flow). Endothelial cell (EC) nuclei are indicated by arrows. Widths of intersomitic vessels (ISVs) with nontransgenic and KRAS^{G12V}-positive cells are indicated with red bars. 48 hpf. Scale bar=20 μm. **B**, Quantification of average diameter of ISVs containing cells expressing the *kdrl*:KRAS^{WT} or *kdrl*:KRAS^{G12V} transgene (+) or in transgene-negative (–) ISVs or in ISVs in uninjected control (UIC) embryos. Kruskal-Wallis test with Dunn multiple comparisons test. **C**, Quantification of the number of EC nuclei in ISVs in *Tg* (*fli1a*:nls-GFP) embryos containing cells expressing the *kdrl*:KRAS^{G12V} transgene (+) or in transgene-negative (–) ISVs. Unpaired Mann-Whitney *U* test; *P*=0.055. **D**, Quantification of ISV cell area (ie, total ISV area divided by the number of *fli1a*:nls-GFP nuclei) in ISVs containing cells expressing the *kdrl*:KRAS^{G12V} transgene (+) or in transgene-negative (–) ISVs. Unpaired Mann-Whitney *U* test. Representative images (**E**) and quantification (**F**) of human umbilical vein endothelial cells electroporated with control or KRAS^{G12V} constructs, together with a LifeAct-GFP construct. Scale bar=40 μm. Unpaired Mann-Whitney *U* test.

the MEK inhibitor, SL327, or an equivalent amount of vehicle (ie, DMSO) at 28 hpf, before the formation of observable shunts, and the prevalence of AV shunts was later assessed at 48 hpf. Importantly, this dose of SL327 does not impair ISV formation (data not shown) but does lower pERK levels (Online Figure XB). We found that SL327 treatment reduced the proportion of KRAS^{G12V}-injected embryos that had shunts between the DA and posterior cardinal vein, demonstrating that KRAS-mediated shunt formation requires MEK activity (Online Figure XC).

Next, we sought to determine whether MEK activity was required to maintain established AV shunts. Zebrafish injected with *kdrl:*EGFP-KRAS^{G12V} were screened for the presence of AV shunts at ≈36 hpf and then embryos were treated with 1 μM SL327 or an equivalent amount of vehicle control (ie, DMSO), and the presence of shunts was assessed 24 hours later (≈60 hpf). While ≈19% of embryos exposed to DMSO for 24 hours had reversal of established shunts, treatment with SL327 rescued this defect in ≈66% of

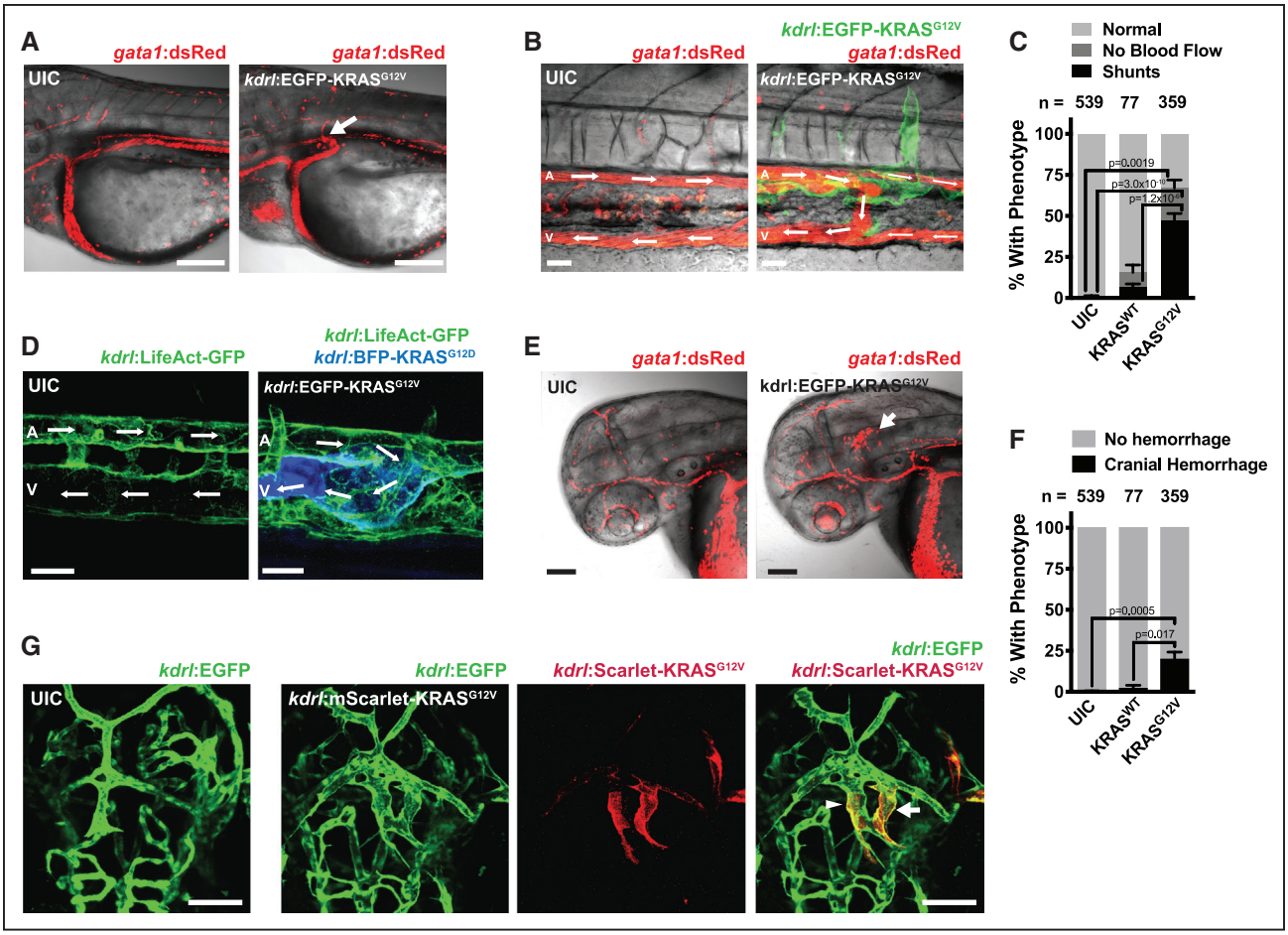

Figure 5. Active KRAS (Kirsten rat sarcoma viral oncogene homologue) expression in the endothelium drives the formation of arteriovenous shunts and cranial hemorrhage.

A, Representative image of an arteriovenous (AV) shunt (indicated by arrow) between the dorsal aorta (DA) and the cardinal vein (CV) in a *Tg*(*gata1*:dsRed) zebrafish embryo injected with *kdrl*:EGFP-KRAS^{G12V}, but not in uninjected controls (UIC). Scale bar=100 µm. 60 hpf. **B**, Representative image of an AV shunt between the DA (A) and posterior CV (V) in the trunk of a *Tg*(*gata1*:dsRed) embryo injected with *kdrl*:EGFP-KRAS^{G12V}, but not in UIC. Blood flow is indicated by arrows. Note that EGFP-KRAS^{G12V}-expressing cells are present at the location of the shunt. Scale bar=30 µm. 64 hpf. **C**, Quantification of AV shunts and no blood flow phenotypes in the trunk of embryos injected with *kdrl*:EYFP-KRAS^{WT}, *kdrl*:EGFP-KRAS^{G12V} or UIC, as assessed under bright field imaging at 48 hpf. Data are mean±SEM of the percentages of phenotypes from multiple independent experiments. The total number of embryos analyzed are indicated above. One-way ANOVA with Tukey's multiple comparisons test. **D**, Representative images of *Tg* (*kdrl*:LifeAct-GFP) embryos injected with a *kdrl*:BFP-KRAS^{G12D} construct or UIC demonstrating an AV shunt and altered actin polymerization. Scale bar=20 µm. 72 hpf. **E**, Representative image of a cranial hemorrhage in a *Tg* (*gata1*:dsRed) embryo injected with *kdrl*:EGFP-KRAS^{G12V} but not in UIC. Scale bar=90 µm. 48 hpf. **F**, Quantification of cranial hemorrhages in embryos injected with *kdrl*:EYFP-KRAS^{WT}, *kdrl*:EGFP-KRAS^{G12V} or UIC, as assessed under bright field at 48 hpf. Data are mean±SEM of the percentages of phenotypes from multiple independent experiments. The total number of embryos analyzed are indicated above. One-way ANOVA with Tukey's multiple comparisons test. **G**, Representative images of cranial blood vessels in *Tg* (*kdrl*:EGFP) embryos injected with *kdrl*:mScarlet-KRAS^{G12V} and in UIC. The arrow indicates an abnormal vascular connection with large lumen and the arrowhead indicates a vessel with an expanded lumen. Scale bar=50 µm. 54 hpf.

embryos (Figure 7A and 7B). To determine the specificity of this response, we treated embryos with established KRAS^{G12V}-induced shunts at 36 hpf with the PI3Ki, LY294002, at a dose (10 µM) that inhibits pAKT levels but does not affect blood flow (Online Figure XD and XE), and assessed shunts 24 hours later (Online Figure XF; Figure 7B). No change in shunt frequency was observed with this treatment.

We next determined if MEK inhibition could also reverse KRAS-induced morphological changes in ISVs. Embryos carrying a *Tg*(*kdrl*:LifeAct-GFP) reporter that were injected with *kdrl*:mScarlet-KRAS^{G12V} displayed enhanced ectopic EC sprouting compared with uninjected controls at ≈36 hpf (Figure 7C). Embryos were then treated with DMSO or SL327 and the same embryos were imaged again later at ≈60 hpf. Ectopic sprouts were still present in *kdrl*:KRAS^{G12V}-expressing embryos treated with DMSO, while vascular morphology appeared to be normalized in SL327-treated embryos (Figure 7C).

Finally, we sought to determine whether inhibition of MEK activity could prevent the formation

ORIGINAL RESEARCH

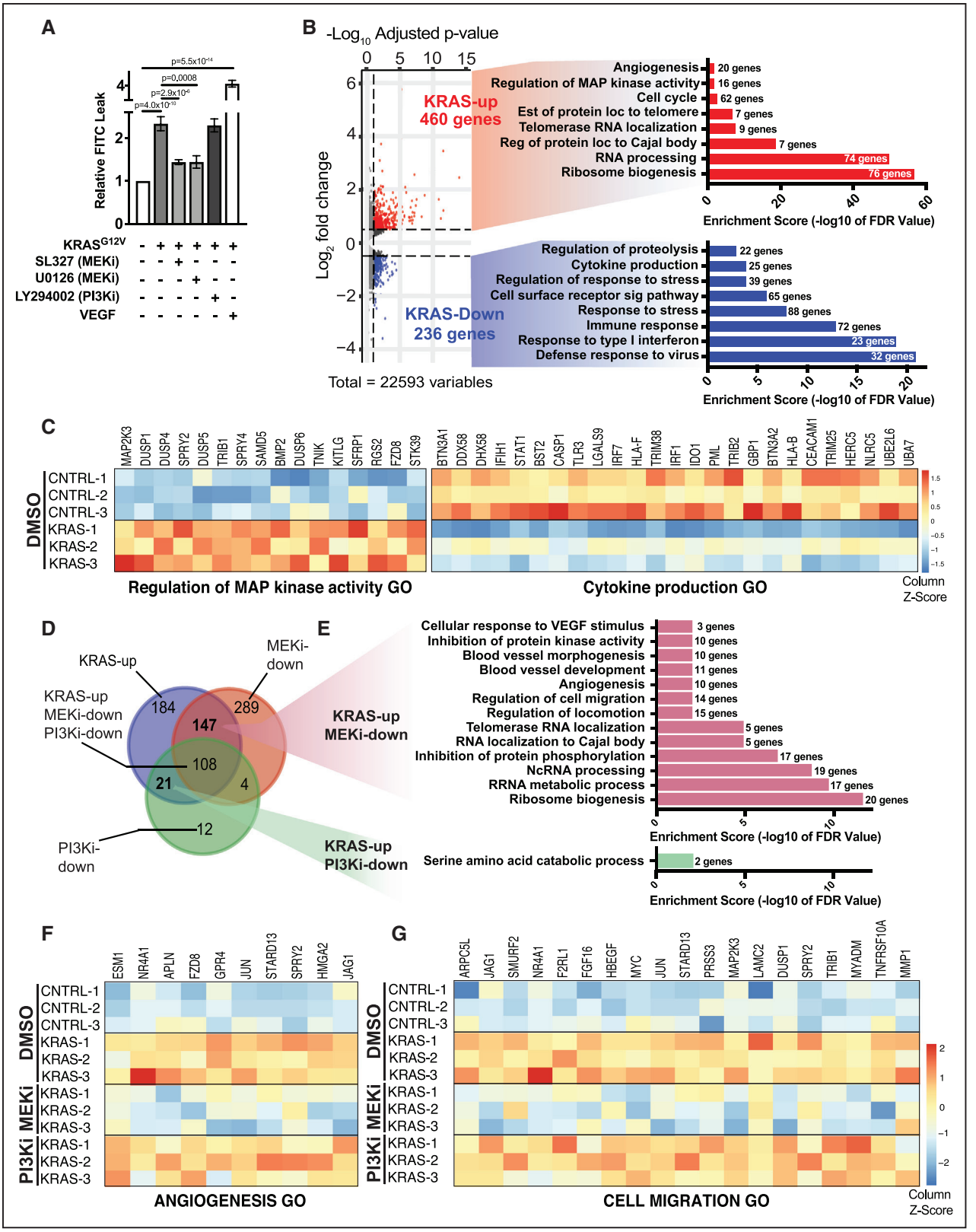

Figure 6. KRAS^{G12V} (Kirsten rat sarcoma viral oncogene homologue)-signaling disrupts endothelial cell (EC) barrier and alters gene regulatory networks in a MEK (mitogen-activated protein kinase kinase 1)-dependent manner.

A, EC barrier was assessed using a transwell leak assay with a FITC-Dextran tracer in HUVECs expressing KRAS^{G12V}±MEK inhibition (MEKi) with SL327 or U0126 or PI3K inhibition (PI3Ki) with LY294002 or control cells (ie, empty vector). VEGF treatment was included as a positive control for EC permeability. n=9 for control, KRAS^{G12V} and KRAS^{G12V}+SL327; n=3 for KRAS^{G12V}+U0126 and KRAS^{G12V}+LY294002; (*Continued*)

of cranial hemorrhages in *kdrl*:KRAS^{G12V}-injected embryos. Indeed, addition of SL327 at ≈28 hpf reduced the percentage of embryos that developed hemorrhage by 48 hpf compared with control embryos (Figure 7D and 7E).

DISCUSSION

AVMs in the brain vasculature are a significant source of morbidity and mortality in children and young adults.[32] New therapies, particularly pharmacological approaches, are desperately needed as existing surgical interventions pose significant risks to patients.[33] It is now apparent that somatic mutations that lead to constitutive activation of the KRAS-MEK pathway are the most common known genetic cause of sporadic bAVMs and occur in the majority of such lesions.[3–7] Yet, the mechanisms whereby this signaling pathway can promote abnormal connections between arteries and veins is poorly understood. Here, we have developed the first animal models of this disease and find that expression of active KRAS (G12V or G12D) in the endothelium is sufficient to drive the formation of bAVMs in mice and zebrafish. Furthermore, we demonstrate in zebrafish that inhibition of MEK can block and even reverse AV shunts. These models will serve as valuable platforms to uncover the molecular mechanisms involved in sporadic bAVM pathogenesis and to develop novel therapies. Critically, the lesions observed in our animal models are analogous to human bAVM pathology, providing strong evidence that activating KRAS mutations are causative of the disease and that MEK inhibition may be a feasible approach for treatment of patients with bAVMs.

While these same KRAS mutations promote proliferation of tumorigenic cells, we demonstrate that expression of activated KRAS in the endothelium does not affect proliferation but instead leads to striking changes in EC phenotype. These phenotypes include ectopic sprouting, increased cell size, disorganization of cell shape, expansion of lumen diameter, and abnormal connections between arteries and veins. While we observed AV shunts, establishment of AV identity did not appear to be altered. Instead, we find increased activation of ETS reporter activity in KRAS-expressing cells and in neighboring ECs in vivo. Given the critical role of ETS factors in regulating angiogenesis, coupled with our previous observation of a VEGF-like transcriptional signature in KRAS expressing cells,[3] and our finding of ectopic sprouting in vivo upon KRAS expression, we suggest that alterations in protrusive and migratory behavior plays a significant, or even causative role in the formation of abnormal connections between arteries and veins. In contrast to other AVM mouse models (eg, Hereditary Hemorrhagic Telangiectasia),[31,34–36] injury or external angiogenic stimuli are not required for AVM formation in adult vessels as KRAS signaling may provide the angiogenic and remodeling cues. Stochastic aberrant connections between arteries and veins or additional physiological cues that remain to be uncovered may contribute to the focal nature of bAVMs in our mouse model (despite widespread expression of mutant KRAS in all ECs).

A characteristic feature of AVMs are their expanded vascular lumens. Of note, a recent immunohistochemistry study demonstrated that KRAS^{G12D} tended to be expressed in ECs of dilated vessels in bAVMs.[4] This matches our observation in zebrafish and mouse models that active KRAS-expressing vessels feature a distinctly large diameter. The mechanisms responsible for the expanded lumen are not yet clear, but we provide evidence that active KRAS signaling leads to enhanced EC size. Identification of the pathways activated downstream of KRAS would help determine the mechanisms underlying KRAS-induced alterations in cell shape and lumen diameter. Given the involvement of blood flow in mediating morphogenic defects in distinct types of vascular malformations,[37,38] it will also be of interest to determine how KRAS-dependent increases in lumen diameter are involved in disease pathogenesis and whether KRAS-mutant cells have abnormal responses to flow.

Although multiple RAS family members are expressed in ECs (ie, *KRAS*, *NRAS*, *HRAS*), it remains unclear why sporadic bAVMs involve activating mutations exclusively in KRAS. Furthermore, mutations in negative regulators

Figure 6 Continued. n=6 for VEGF. One-way ANOVA with Tukey's multiple comparisons test. For simplicity, not all significant comparisons are indicated. PI3Ki was not able to rescue KRAS-dependent leak; *P*=0.9999. **B**, Volcano-plot of differentially expressed genes in HUVECs expressing KRAS^{G12V} compared with empty vector control. Associated select GO terms (with enrichment score below and number of genes to the right) for genes up-regulated by KRAS^{G12V} are shown in red, while those downregulated are shown in blue. **C**, Heat maps of differentially expressed transcripts detected by RNA-seq in 2 representative GO categories are shown (n=3 biological replicates). **D**, A Venn diagram shows the overlap between genes that are differentially up-regulated in HUVECs expressing KRAS^{G12V} compared with empty vector control following treatment with vehicle (DMSO), PI3Ki (LY294002), or MEKi (U01236). A small subset of KRAS^{G12V} upregulated targets (460 total genes) are uniquely affected by PI3Ki (21 genes), although MEKi affects a larger cohort of these KRAS-induced transcripts (147 genes). Significant genes in the Venn diagram were included if they displayed a Benjamini–Hochberg adjusted *P*-value of <0.1 and a log2 (fold change) >0.5. **E**, Associated select GO terms of MEKi- and PI3Ki-sensitive genes. **F** and **G**, Heat maps of differentially expressed transcripts detected by RNA-seq in 2 representative GO categories. KRAS^{G12V}-induced transcripts in these GO categories are not downregulated following PI3Ki but are decreased following MEKi. See Online Table II for gene list of KRAS-induced, MEK-dependent and PI3K-dependent transcripts, along with a full list of linked Gene Ontology categories.

ORIGINAL RESEARCH

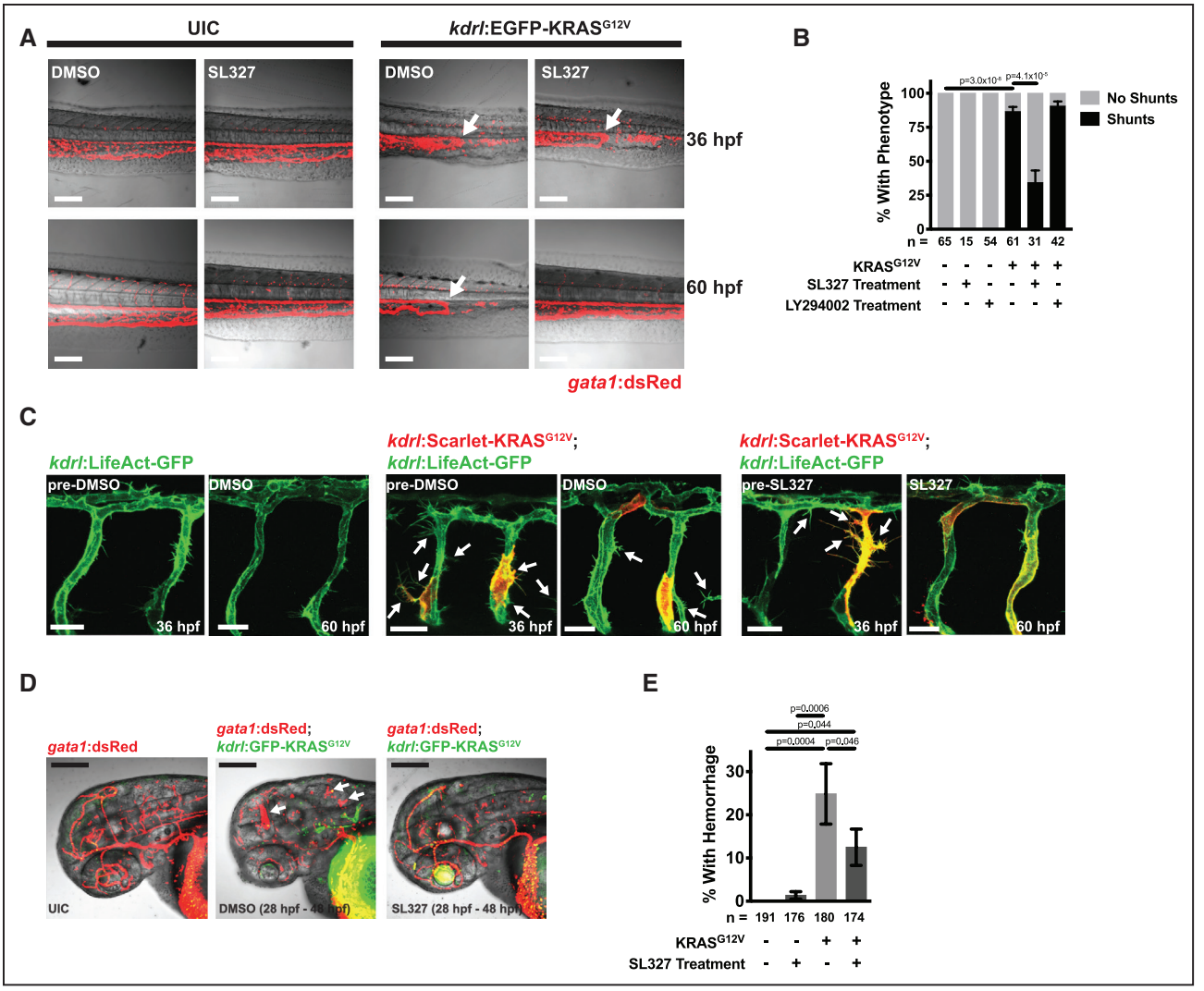

Figure 7. MEK (mitogen-activated protein kinase kinase 1) inhibition can rescue phenotypes caused by active KRAS (Kirsten rat sarcoma viral oncogene homologue) signaling in endothelial cells.

A, Representative images of *Tg*(*gata1*:dsRed) embryos, that were either uninjected (ie, UIC) or were injected with *kdrl*:EGFP-KRAS^{G12V}. Embryos were imaged at 36 hpf to identify embryos with AV shunts, at which point these embryos were exposed to either DMSO or 1 μM of the MEK inhibitor, SL327. The same embryos were imaged at 60 hpf. Scale bar=40 μm. **B**, Quantification of phenotypes after 24 h of SL327 (1 μM), LY294002 (PI3K inhibitor, 10 μM), or vehicle (ie, DMSO) treatment. All KRAS^{G12V} embryos had shunts at the beginning of treatment. Data are mean±SEM of the percentages of phenotypes from 5 (SL327) or 4 (LY294002) independent experiments. The SL327 and LY294002 treatments were performed in different experiments and data are combined in one graph for visualization purposes, but analysis was done separately. The total number of embryos analyzed are indicated below. One-way ANOVA with Tukey's multiple comparison test. For simplicity, not all significant comparisons are indicated. PI3K was not able to rescue established shunts; P=0.816. See Online Figure X for more data on LY294002 treatment. **C**, Representative images of *Tg*(*kdrl*:LifeAct-GFP) embryos injected with *kdrl*:mScarlet-KRAS^{G12V} or UIC. Images were taken at 36 hpf and embryos were treated with 1 μM SL327 or DMSO control and imaging was then repeated on the same embryos at 60 hpf. *kdrl*:mScarlet-KRAS^{G12V}-injected embryos had ectopic sprouts (indicated by arrows) and these continued to be present at 60 hpf in embryos exposed to DMSO, but this phenotype was normalized by treatment with SL327. Scale bar=20 μm. **D**, Hemorrhage phenotype in *Tg*(*gata1*:dsRed) embryos treated with DMSO or 1 μM SL327 from 28 to 48 hpf. Hemorrhages are indicated by arrows. Scale bar=200 μm. **E**, Quantification of the percentage of embryos with cranial hemorrhage (mean±SEM) from 6 independent experiments. The total number of embryos analyzed are indicated below. Statistical significance was determined by one-way ANOVA with Tukey multiple comparison test.

of RAS signaling (eg, *RASA1*/p120-RasGAP) are associated with capillary-malformation arteriovenous malformation (CM-AVM1) in humans[39] and a subset of these patients present with intracranial AVMs,[40] and while mouse models present with vascular and lymphatic defects,[41–45] they did not feature bAVMs. Interestingly, activating NRAS variants have been observed in a highly aggressive vascular malformation of the lymphatics, known as lymphangiomatosis,[46,47] and HRAS gain of function variants have been observed in ECs isolated from a patient with an extracranial AVM.[48] A recent transgenic mouse model in which active HRAS was expressed in the postnatal endothelium showed that the abnormal and

sustained activation of the RAS pathway can drive vascular defects, including dilation of capillary vessels and diffuse hemorrhage in the brain, but not other organs.[49] It is notable, however, that these phenotypes seem to be distinct from those observed following KRAS activation in the endothelium, as no bAVMs were noted. This points to unique roles for RAS proteins in vessel morphogenesis and homeostasis, which requires further exploration.

As KRAS is difficult to target pharmacologically, most therapies for treating KRAS-mutant cancers have focused on targeting downstream signaling molecules, including MEK.[50–54] We are encouraged by our finding that inhibition of MEK signaling can reverse already-established AV shunts in KRAS-expressing zebrafish. It will be important to determine whether advanced lesions in the mouse brain—which feature a tangled nidus—can be reversed through inhibiting effectors that act downstream of KRAS signaling. If the abnormal vessel architecture that we observed requires continual KRAS activity and MEK/ERK signaling, similar to addiction to KRAS signaling in cancer,[55] then pharmacological blockade of these downstream effectors may offer hope to patients suffering from sporadic bAVM. Indeed, recent studies using animal models of venous and lymphatic malformations and small pilot studies in humans have shown that pharmacological blockade of aberrant signaling pathways may be a feasible therapeutic approach for managing vascular malformations.[16,56,57] However, whether MEK inhibition can reverse advanced cerebrovascular lesions in humans, which may have been present for decades and have undergone extensive remodeling due to chronic responses to altered blood flow and inflammation, remains to be seen. Notably, a recent case report of efficacy of MEK inhibitor therapy (trametinib) in reducing the size and vessel caliber of a skin AVM that contained activating MAP2K1 mutations, provides some optimism.[58]

Taken together, we demonstrate that KRAS gain of function mutations in ECs can drive abnormal vascular morphology and AVMs in mouse and zebrafish models and that these lesions can be reversed by inhibiting MEK signaling. Furthermore, unlike other genetic animal models, expression of active KRAS in adult ECs is sufficient to induce bAVM formation. These findings provide new insight into sporadic bAVMs and offer hope that therapeutic approaches can be utilized to negate KRAS-mediated alterations in vessel morphology.

ARTICLE INFORMATION

Received December 6, 2019; revision received June 2, 2020; accepted June 16, 2020.

Affiliations

From the Toronto General Hospital Research Institute (J.E.F., E.B., D.G., P.V.D., Z.C.), Peter Munk Cardiac Centre (J.E.F.), Krembil Research Institute (I.R.), and Division of Neurosurgery, Sprott Department of Surgery (I.R.), University Health Network, Canada; Department of Laboratory Medicine and Pathobiology (J.E.F., D.G.) and Department of Surgery (I.R.), University of Toronto, Canada; Cardiovascular Research Institute (C.P.F.S., A.M.H., M.C.G., M.C., K.B.D.R., J.D.W.) and Department of Molecular Physiology and Biophysics (C.P.F.S., A.M.H., M.C.G., M.C., K.B.D.R., T.S.S., C.S.W., J.D.W.), Graduate Program in Developmental Biology (M.C.G., J.D.W.), and Advanced Technology Cores (T.S.S., C.S.W.), Baylor College of Medicine, Houston, TX.

Acknowledgments

We thank Kate Wythe for the model graphics in Figures 1A, 2A, and 3A, and the graphic abstract. The authors also thank the Optical Imaging and Vital Microscopy core, run by Dr Mary Dickinson and Mr Jason Kirk, for assistance with both normal confocal and lightsheet imaging, data analysis, and 3-dimensional image reconstruction. J.E. Fish and J.D. Wythe conceptualized the study; J.E. Fish, C.P. Flores Suarez, E. Boudreau, A.M. Herman, and J.D. Wythe designed experiments; C.P. Flores Suarez, E. Boudreau, A.M. Herman, M.C. Gutierrez and P.V. DiStefano conducted the majority of experiments with help from D. Gustafson, M. Cui, Z. Chen, T.S. Schexnayder, C.S. Ward, and K.B. De Ruiz; M.C. Gutierrez and J.D. Wythe performed the bioinformatic analysis; all authors acquired data; J.E. Fish, C.P. Flores Suarez, E. Boudreau, A.M. Herman, M.C. Gutierrez, C.S. Ward, and J.D. Wythe analyzed the data; J.E. Fish and J.D. Wythe wrote the original draft of the manuscript; J.E. Fish, A.M. Herman, P.V. DiStefano, M.C. Gutierrez, D. Gustafson, C.S. Ward, I. Radovanovic, and J.D. Wythe secured funding; all authors edited and approved the manuscript.

Sources of Funding

T.S. Schexnayder and C.S. Ward in the Mouse Metabolism and Phenotyping Core at Baylor College of Medicine were supported with funding from National Institutes of Health (UM1HG006348, R01DK114356, R01HL130249). J.E. Fish is supported by a Canada Research Chair from the Canadian Institutes of Health Research (CIHR) and his lab received infrastructure funding from the Canada Foundation for Innovation, the John R. Evans Leaders Fund and the Ontario Research Fund. Research in the Fish laboratory is supported by a Project Grant from CIHR (PJT 155922), the US Department of Defense (W81XWH-18-1-0351) and a Medicine by Design Team Project Award, which receives funding from the Canada First Research Excellence Fund. A.M. Herman was supported by the National Institutes of Health (5T32HL007676-27, 5T32HL007676-28) and American Heart Association Postdoctoral Award (19POST34430008). P.V. DiStefano was supported by a post-doctoral fellowship from the Toronto General Hospital Research Institute. D. Gustafson is supported by a Canada Graduate Scholarship from CIHR. M.C. Gutierrez was supported by an American Heart Association Predoctoral Award (19PRE34410104). J.D. Wythe is supported by institutional startup funds from the Cardiovascular Research Institute at Baylor College of Medicine, the Caroline Wiess Law Fund for Research in Molecular Medicine, the Curtis and Doris K. Hankamer Foundation Basic Research Fund, and the ARCO Foundation Young Teacher-Investigator Award. J.D. Wythe and work within the Wythe laboratory is supported by the Department of Defense (W81XWH-18-1-0350) and CIHR (PJT 155922).

Disclosures

None.

Supplemental Materials

Detailed Methods
Online Figures I–XIII
Uncropped Western Blots
Online Tables I–V
Online Videos I–IV
Online File I
References[59–83]
Online RStudio File

REFERENCES

1. Solomon RA, Connolly ES Jr. Arteriovenous malformations of the brain. *N Engl J Med.* 2017;376:1859–1866. doi: 10.1056/NEJMra1607407
2. Yun JH, Kwon DH, Lee EJ, Lee DH, Ahn JS, Kwun BD. New nidus formation adjacent to the target site of an arteriovenous malformation treated by Gamma Knife surgery. *J Neurosurg.* 2012;117(suppl):120–125. doi: 10.3171/2012.8.GKS12994
3. Nikolaev SI, Vetiska S, Bonilla X, Boudreau E, Jauhiainen S, Rezai Jahromi B, Khyzha N, DiStefano PV, Suutarinen S, Kiehl TR, et al. Somatic activating KRAS mutations in arteriovenous malformations of the brain. *N Engl J Med.* 2018;378:250–261. doi: 10.1056/NEJMoa1709449
4. Oka M, Kushamae M, Aoki T, Yamaguchi T, Kitazato K, Abekura Y, Kawamata T, Mizutani T, Miyamoto S, Takagi Y. KRAS G12D or G12V

mutation in human brain arteriovenous malformations. *World Neurosurg*. 2019;126:e1365–e1373. doi: 10.1016/j.wneu.2019.03.105
5. Priemer DS, Vortmeyer AO, Zhang S, Chang HY, Curless KL, Cheng L. Activating KRAS mutations in arteriovenous malformations of the brain: frequency and clinicopathologic correlation. *Hum Pathol*. 2019;89:33–39. doi: 10.1016/j.humpath.2019.04.004
6. Hong T, Yan Y, Li J, Radovanovic I, Ma X, Shao YW, Yu J, Ma Y, Zhang P, Ling F, et al. High prevalence of KRAS/BRAF somatic mutations in brain and spinal cord arteriovenous malformations. *Brain*. 2019;142:23–34. doi: 10.1093/brain/awy307
7. Al-Olabi L, Polubothu S, Dowsett K, Andrews KA, Stadnik P, Joseph AP, Knox R, Pittman A, Clark G, Baird W, et al. Mosaic RAS/MAPK variants cause sporadic vascular malformations which respond to targeted therapy. *J Clin Invest*. 2018;128:1496–1508. doi: 10.1172/JCI98589
8. Serebriiskii IG, Connelly C, Frampton G, Newberg J, Cooke M, Miller V, Ali S, Ross JS, Handorf E, Arora S, et al. Comprehensive characterization of RAS mutations in colon and rectal cancers in old and young patients. *Nat Commun*. 2019;10:3722. doi: 10.1038/s41467-019-11530-0
9. Lapinski PE, Doosti A, Salato V, North P, Burrows PE, King PD. Somatic second hit mutation of RASA1 in vascular endothelial cells in capillary malformation-arteriovenous malformation. *Eur J Med Genet*. 2018;61:11–16. doi: 10.1016/j.ejmg.2017.10.004
10. Limaye N, Wouters V, Uebelhoer M, Tuominen M, Wirkkala R, Mulliken JB, Eklund L, Boon LM, Vikkula M. Somatic mutations in angiopoietin receptor gene TEK cause solitary and multiple sporadic venous malformations. *Nat Genet*. 2009;41:118–124. doi: 10.1038/ng.272
11. Limaye N, Kangas J, Mendola A, Godfraind C, Schlögel MJ, Helaers R, Eklund L, Boon LM, Vikkula M. Somatic activating PIK3CA mutations cause venous malformation. *Am J Hum Genet*. 2015;97:914–921. doi: 10.1016/j.ajhg.2015.11.011
12. Shirley MD, Tang H, Gallione CJ, Baugher JD, Frelin LP, Cohen B, North PE, Marchuk DA, Comi AM, Pevsner J. Sturge-Weber syndrome and port-wine stains caused by somatic mutation in GNAQ. *N Engl J Med*. 2013;368:1971–1979. doi: 10.1056/NEJMoa1213507
13. Huang L, Couto JA, Pinto A, Alexandrescu S, Madsen JR, Greene AK, Sahin M, Bischoff J. Somatic GNAQ mutation is enriched in brain endothelial cells in Sturge-Weber syndrome. *Pediatr Neurol*. 2017;67:59–63. doi: 10.1016/j.pediatrneurol.2016.10.010
14. Hammer J, Seront E, Duez S, Dupont S, Van Damme A, Schmitz S, Hoyoux C, Chopinet C, Clapuyt P, Hammer F, et al. Sirolimus is efficacious in treatment for extensive and/or complex slow-flow vascular malformations: a monocentric prospective phase II study. *Orphanet J Rare Dis*. 2018;13:191. doi: 10.1186/s13023-018-0934-z
15. Li X, Cai Y, Goines J, Pastura P, Brichta L, Lane A, Le Cras TD, Boscolo E. Ponatinib combined with rapamycin causes regression of murine venous malformation. *Arterioscler Thromb Vasc Biol*. 2019;39:496–512. doi: 10.1161/ATVBAHA.118.312315
16. Boscolo E, Limaye N, Huang L, Kang KT, Soblet J, Uebelhoer M, Mendola A, Natynki M, Seront E, Dupont S, et al. Rapamycin improves TIE2-mutated venous malformation in murine model and human subjects. *J Clin Invest*. 2015;125:3491–3504. doi: 10.1172/JCI76004
17. Hong CC, Peterson QP, Hong JY, Peterson RT. Artery/vein specification is governed by opposing phosphatidylinositol-3 kinase and MAP kinase/ERK signaling. *Curr Biol*. 2006;16:1366–1372. doi: 10.1016/j.cub.2006.05.046
18. Deng Y, Larrivée B, Zhuang ZW, Atri D, Moraes F, Prahst C, Eichmann A, Simons M. Endothelial RAF1/ERK activation regulates arterial morphogenesis. *Blood*. 2013;121:3988–96, S1. doi: 10.1182/blood-2012-12-474601
19. Wythe JD, Dang LT, Devine WP, Boudreau E, Artap ST, He D, Schachterle W, Stainier DY, Oettgen P, Black BL, et al. ETS factors regulate Vegf-dependent arterial specification. *Dev Cell*. 2013;26:45–58. doi: 10.1016/j.devcel.2013.06.007
20. Shin M, Beane TJ, Quillien A, Male I, Zhu LJ, Lawson ND. Vegfa signals through ERK to promote angiogenesis, but not artery differentiation. *Development*. 2016;143:3796–3805. doi: 10.1242/dev.137919
21. Fish JE, Cantu Gutierrez M, Dang LT, Khyzha N, Chen Z, Veitch S, Cheng HS, Khor M, Antounians L, Njock MS, et al. Dynamic regulation of VEGF-inducible genes by an ERK/ERG/p300 transcriptional network. *Development*. 2017;144:2428–2444. doi: 10.1242/dev.146050
22. Yaeger R, Corcoran RB. Targeting alterations in the RAF-MEK pathway. *Cancer Discov*. 2019;9:329–341. doi: 10.1158/2159-8290.CD-18-1321
23. Wang Y, Nakayama M, Pitulescu ME, Schmidt TS, Bochenek ML, Sakakibara A, Adams S, Davy A, Deutsch U, Lüthi U, et al. Ephrin-B2 controls VEGF-induced angiogenesis and lymphangiogenesis. *Nature*. 2010;465:483–486. doi: 10.1038/nature09002
24. Jackson EL, Willis N, Mercer K, Bronson RT, Crowley D, Montoya R, Jacks T, Tuveson DA. Analysis of lung tumor initiation and progression using conditional expression of oncogenic K-ras. *Genes Dev*. 2001;15:3243–3248. doi: 10.1101/gad.943001
25. Murphy PA, Lam MT, Wu X, Kim TN, Vartanian SM, Bollen AW, Carlson TR, Wang RA. Endothelial Notch4 signaling induces hallmarks of brain arteriovenous malformations in mice. *Proc Natl Acad Sci U S A*. 2008;105:10901–10906. doi: 10.1073/pnas.0802743105
26. Ridder DA, Lang MF, Salinin S, Röderer JP, Struss M, Maser-Gluth C, Schwaninger M. TAK1 in brain endothelial cells mediates fever and lethargy. *J Exp Med*. 2011;208:2615–2623. doi: 10.1084/jem.20110398
27. Mahmoud M, Allinson KR, Zhai Z, Oakenfull R, Ghandi P, Adams RH, Fruttiger M, Arthur HM. Pathogenesis of arteriovenous malformations in the absence of endoglin. *Circ Res*. 2010;106:1425–1433. doi: 10.1161/CIRCRESAHA.109.211037
28. Tual-Chalot S, Mahmoud M, Allinson KR, Redgrave RE, Zhai Z, Oh SP, Fruttiger M, Arthur HM. Endothelial depletion of Acvrl1 in mice leads to arteriovenous malformations associated with reduced endoglin expression. *PLoS One*. 2014;9:e98646. doi: 10.1371/journal.pone.0098646
29. Nielsen CM, Huang L, Murphy PA, Lawton MT, Wang RA. Mouse Models of Cerebral Arteriovenous Malformation. *Stroke*. 2016;47:293–300. doi: 10.1161/STROKEAHA.115.002869
30. Park SO, Wankhede M, Lee YJ, Choi EJ, Fliess N, Choe SW, Oh SH, Walter G, Raizada MK, Sorg BS, et al. Real-time imaging of de novo arteriovenous malformation in a mouse model of hereditary hemorrhagic telangiectasia. *J Clin Invest*. 2009;119:3487–3496. doi: 10.1172/JCI39482
31. Chen W, Sun Z, Han Z, Jun K, Camus M, Wankhede M, Mao L, Arnold T, Young WL, Su H. De novo cerebrovascular malformation in the adult mouse after endothelial Alk1 deletion and angiogenic stimulation. *Stroke*. 2014;45:900–902. doi: 10.1161/STROKEAHA.113.003655
32. Leblanc GG, Golanov E, Awad IA, Young WL; Biology of Vascular Malformations of the Brain NINDS Workshop Collaborators. Biology of vascular malformations of the brain. *Stroke*. 2009;40:e694–e702. doi: 10.1161/STROKEAHA.109.563692
33. Lawton MT, Rutledge WC, Kim H, Stapf C, Whitehead KJ, Li DY, Krings T, terBrugge K, Kondziolka D, Morgan MK, et al. Brain arteriovenous malformations. *Nat Rev Dis Primers*. 2015;1:15008. doi: 10.1038/nrdp.2015.8
34. Xu B, Wu YQ, Huey M, Arthur HM, Marchuk DA, Hashimoto T, Young WL, Yang GY. Vascular endothelial growth factor induces abnormal microvasculature in the endoglin heterozygous mouse brain. *J Cereb Blood Flow Metab*. 2004;24:237–244. doi: 10.1097/01.WCB.0000107730.66603.51
35. Hao Q, Zhu Y, Su H, Shen F, Yang GY, Kim H, Young WL. VEGF induces more severe cerebrovascular dysplasia in endoglin than in Alk1 mice. *Transl Stroke Res*. 2010;1:197–201. doi: 10.1007/s12975-010-0020-x
36. Choi EJ, Walker EJ, Shen F, Oh SP, Arthur HM, Young WL, Su H. Minimal homozygous endothelial deletion of Eng with VEGF stimulation is sufficient to cause cerebrovascular dysplasia in the adult mouse. *Cerebrovasc Dis*. 2012;33:540–547. doi: 10.1159/000337762
37. Sugden WW, Meissner R, Aegerter-Wilmsen T, Tsaryk R, Leonard EV, Bussmann J, Hamm MJ, Herzog W, Jin Y, Jakobsson L, et al. Endoglin controls blood vessel diameter through endothelial cell shape changes in response to haemodynamic cues. *Nat Cell Biol*. 2017;19:653–665. doi: 10.1038/ncb3528
38. Rochon ER, Menon PG, Roman BL. Alk1 controls arterial endothelial cell migration in lumenized vessels. *Development*. 2016;143:2593–2602. doi: 10.1242/dev.135392
39. Eerola I, Boon LM, Mulliken JB, Burrows PE, Dompmartin A, Watanabe S, Vanwijck R, Vikkula M. Capillary malformation-arteriovenous malformation, a new clinical and genetic disorder caused by RASA1 mutations. *Am J Hum Genet*. 2003;73:1240–1249. doi: 10.1086/379793
40. Revencu N, Boon LM, Mulliken JB, Enjolras O, Cordisco MR, Burrows PE, Clapuyt P, Hammer F, Dubois J, Baselga E, et al. Parkes Weber syndrome, vein of Galen aneurysmal malformation, and other fast-flow vascular anomalies are caused by RASA1 mutations. *Hum Mutat*. 2008;29:959–965. doi: 10.1002/humu.20746
41. Chen D, Teng JM, North PE, Lapinski PE, King PD. RASA1-dependent cellular export of collagen IV controls blood and lymphatic vascular development. *J Clin Invest*. 2019;129:3545–3561. doi: 10.1172/JCI124917
42. Henkemeyer M, Rossi DJ, Holmyard DP, Puri MC, Mbamalu G, Harpal K, Shih TS, Jacks T, Pawson T. Vascular system defects and neuronal apoptosis in mice lacking ras GTPase-activating protein. *Nature*. 1995;377:695–701. doi: 10.1038/377695a0

43. Lapinski PE, Kwon S, Lubeck BA, Wilkinson JE, Srinivasan RS, Sevick-Muraca E, King PD. RASA1 maintains the lymphatic vasculature in a quiescent functional state in mice. *J Clin Invest*. 2012;122:733–747. doi: 10.1172/JCI46116
44. Lapinski PE, Lubeck BA, Chen D, Doosti A, Zawieja SD, Davis MJ, King PD. RASA1 regulates the function of lymphatic vessel valves in mice. *J Clin Invest*. 2017;127:2569–2585. doi: 10.1172/JCI89607
45. Lubeck BA, Lapinski PE, Bauler TJ, Oliver JA, Hughes ED, Saunders TL, King PD. Blood vascular abnormalities in Rasa1(R780Q) knockin mice: implications for the pathogenesis of capillary malformation-arteriovenous malformation. *Am J Pathol*. 2014;184:3163–3169. doi: 10.1016/j.ajpath.2014.08.018
46. Barclay SF, Inman KW, Luks VL, McIntyre JB, Al-Ibraheemi A, Church AJ, Perez-Atayde AR, Mangray S, Jeng M, Kreimer SR, et al. A somatic activating NRAS variant associated with kaposiform lymphangiomatosis. *Genet Med*. 2019;21:1517–1524. doi: 10.1038/s41436-018-0390-0
47. Manevitz-Mendelson E, Leichner GS, Barel O, Davidi-Avrahami I, Ziv-Strasser L, Eyal E, Pessach I, Rimon U, Barzilai A, Hirshberg A, et al. Somatic NRAS mutation in patient with generalized lymphatic anomaly. *Angiogenesis*. 2018;21:287–298. doi: 10.1007/s10456-018-9595-8
48. Konczyk DJ, Goss JA, Smits PJ, Huang AY, Al-Ibraheemi A, Sudduth CL, Warman ML, Greene AK. Arteriovenous malformation associated with a HRAS mutation. *Hum Genet*. 2019;138:1419–1421. doi: 10.1007/s00439-019-02072-y
49. Li QF, Decker-Rockefeller B, Bajaj A, Pumiglia K. Activation of Ras in the vascular endothelium induces brain vascular malformations and hemorrhagic stroke. *Cell Rep*. 2018;24:2869–2882. doi: 10.1016/j.celrep.2018.08.025
50. Martinelli E, Morgillo F, Troiani T, Ciardiello F. Cancer resistance to therapies against the EGFR-RAS-RAF pathway: the role of MEK. *Cancer Treat Rev*. 2017;53:61–69. doi: 10.1016/j.ctrv.2016.12.001
51. Merchant M, Moffat J, Schaefer G, Chan J, Wang X, Orr C, Cheng J, Hunsaker T, Shao L, Wang SJ, et al. Combined MEK and ERK inhibition overcomes therapy-mediated pathway reactivation in RAS mutant tumors. *PLoS One*. 2017;12:e0185862. doi: 10.1371/journal.pone.0185862
52. Jessen WJ, Miller SJ, Jousma E, Wu J, Rizvi TA, Brundage ME, Eaves D, Widemann B, Kim MO, Dombi E, et al. MEK inhibition exhibits efficacy in human and mouse neurofibromatosis tumors. *J Clin Invest*. 2013;123:340–347. doi: 10.1172/JCI60578
53. Wang MT, Fer N, Galeas J, Collisson EA, Kim SE, Sharib J, McCormick F. Blockade of leukemia inhibitory factor as a therapeutic approach to KRAS driven pancreatic cancer. *Nat Commun*. 2019;10:3055. doi: 10.1038/s41467-019-11044-9
54. Tetsu O, McCormick F. ETS-targeted therapy: can it substitute for MEK inhibitors? *Clin Transl Med*. 2017;6:16. doi: 10.1186/s40169-017-0147-4
55. Luo J, Solimini NL, Elledge SJ. Principles of cancer therapy: oncogene and non-oncogene addiction. *Cell*. 2009;136:823–837. doi: 10.1016/j.cell.2009.02.024
56. Li D, March ME, Gutierrez-Uzquiza A, Kao C, Seiler C, Pinto E, Matsuoka LS, Battig MR, Bhoj EJ, Wenger TL, et al. ARAF recurrent mutation causes central conducting lymphatic anomaly treatable with a MEK inhibitor. *Nat Med*. 2019;25:1116–1122. doi: 10.1038/s41591-019-0479-2
57. Triana P, Dore M, Cerezo VN, Cervantes M, Sánchez AV, Ferrero MM, González MD, Lopez-Gutierrez JC. Sirolimus in the treatment of vascular anomalies. *Eur J Pediatr Surg*. 2017;27:86–90. doi: 10.1055/s-0036-1593383
58. Lekwuttikarn R, Lim YH, Admani S, Choate KA, Teng JMC. Genotype-guided medical treatment of an arteriovenous malformation in a child. *JAMA Dermatol*. 2019;155:256–257. doi: 10.1001/jamadermatol.2018.4653
59. Villefranc JA, Amigo J, Lawson ND. Gateway compatible vectors for analysis of gene function in the zebrafish. *Dev Dyn*. 2007;236:3077–3087. doi: 10.1002/dvdy.21354
60. Zhou Y, Cashman TJ, Nevis KR, Obregon P, Carney SA, Liu Y, Gu A, Mosimann C, Sondalle S, Peterson RE, et al. Latent TGF-β binding protein 3 identifies a second heart field in zebrafish. *Nature*. 2011;474:645–648. doi: 10.1038/nature10094
61. Nagai T, Ibata K, Park ES, Kubota M, Mikoshiba K, Miyawaki A. A variant of yellow fluorescent protein with fast and efficient maturation for cell-biological applications. *Nat Biotechnol*. 2002;20:87–90. doi: 10.1038/nbt0102-87
62. Zhao L, Borikova AL, Ben-Yair R, Guner-Ataman B, MacRae CA, Lee RT, Burns CG, Burns CE. Notch signaling regulates cardiomyocyte proliferation during zebrafish heart regeneration. *Proc Natl Acad Sci U S A*. 2014;111:1403–1408. doi: 10.1073/pnas.1311705111
63. Kwan KM, Fujimoto E, Grabher C, Mangum BD, Hardy ME, Campbell DS, Parant JM, Yost HJ, Kanki JP, Chien CB. The Tol2kit: a multisite gateway-based construction kit for Tol2 transposon transgenesis constructs. *Dev Dyn*. 2007;236:3088–3099. doi: 10.1002/dvdy.21343
64. Birnbaum RY, Clowney EJ, Agamy O, Kim MJ, Zhao J, Yamanaka T, Pappalardo Z, Clarke SL, Wenger AM, Nguyen L, et al. Coding exons function as tissue-specific enhancers of nearby genes. *Genome Res*. 2012;22:1059–1068. doi: 10.1101/gr.133546.111
65. Mo A, Mukamel EA, Davis FP, Luo C, Henry GL, Picard S, Urich MA, Nery JR, Sejnowski TJ, Lister R, et al. Epigenomic signatures of neuronal diversity in the mammalian brain. *Neuron*. 2015;86:1369–1384. doi: 10.1016/j.neuron.2015.05.018
66. Liu J, Krautzberger AM, Sui SH, Hofmann OM, Chen Y, Baetscher M, Grgic I, Kumar S, Humphreys BD, Humphreys B, et al. Cell-specific translational profiling in acute kidney injury. *J Clin Invest*. 2014;124:1242–1254. doi: 10.1172/JCI72126
67. Madisen L, Zwingman TA, Sunkin SM, Oh SW, Zariwala HA, Gu H, Ng LL, Palmiter RD, Hawrylycz MJ, Jones AR, et al. A robust and high-throughput Cre reporting and characterization system for the whole mouse brain. *Nat Neurosci*. 2010;13:133–140. doi: 10.1038/nn.2467
68. Hayashi S, McMahon AP. Efficient recombination in diverse tissues by a tamoxifen-inducible form of Cre: a tool for temporally regulated gene activation/inactivation in the mouse. *Dev Biol*. 2002;244:305–318. doi: 10.1006/dbio.2002.0597
69. Zudaire E, Gambardella L, Kurcz C, Vermeren S. A computational tool for quantitative analysis of vascular networks. *PLoS One*. 2011;6:e27385. doi: 10.1371/journal.pone.0027385
70. Respress JL, Wehrens XH. Transthoracic echocardiography in mice. *J Vis Exp*. 2010:1738.
71. Jin SW, Beis D, Mitchell T, Chen JN, Stainier DY. Cellular and molecular analyses of vascular tube and lumen formation in zebrafish. *Development*. 2005;132:5199–5209. doi: 10.1242/dev.02087
72. Traver D, Paw BH, Poss KD, Penberthy WT, Lin S, Zon LI. Transplantation and in vivo imaging of multilineage engraftment in zebrafish bloodless mutants. *Nat Immunol*. 2003;4:1238–1246. doi: 10.1038/ni1007
73. Proulx K, Lu A, Sumanas S. Cranial vasculature in zebrafish forms by angioblast cluster-derived angiogenesis. *Dev Biol*. 2010;348:34–46. doi: 10.1016/j.ydbio.2010.08.036
74. Parsons MJ, Pisharath H, Yusuff S, Moore JC, Siekmann AF, Lawson N, Leach SD. Notch-responsive cells initiate the secondary transition in larval zebrafish pancreas. *Mech Dev*. 2009;126:898–912. doi: 10.1016/j.mod.2009.07.002
75. Vanhollebeke B, Stone OA, Bostaille N, Cho C, Zhou Y, Maquet E, Gauquier A, Cabochette P, Fukuhara S, Mochizuki N, et al. Tip cell-specific requirement for an atypical Gpr124- and Reck-dependent Wnt/beta-catenin pathway during brain angiogenesis. *Elife*. 2015;4:e06489.
76. Roman BL, Pham VN, Lawson ND, Kulik M, Childs S, Lekven AC, Garrity DM, Moon RT, Fishman MC, Lechleider RJ, et al. Disruption of acvrl1 increases endothelial cell number in zebrafish cranial vessels. *Development*. 2002;129:3009–3019.
77. Patro R, Duggal G, Love MI, Irizarry RA, Kingsford C. Salmon provides fast and bias-aware quantification of transcript expression. *Nat Methods*. 2017;14:417–419. doi: 10.1038/nmeth.4197
78. Soneson C, Love MI, Robinson MD. Differential analyses for RNA-seq: transcript-level estimates improve gene-level inferences. *F1000Res*. 2015;4:1521. doi: 10.12688/f1000research.7563.2
79. Love MI, Huber W, Anders S. Moderated estimation of fold change and dispersion for RNA-seq data with DESeq2. *Genome Biol*. 2014;15:550. doi: 10.1186/s13059-014-0550-8
80. Blighe K, Rana S, Lewis M. EnhancedVolcano: Publication-ready volcano plots with enhanced colouring and labeling. R package version 152 https://githubcom/kevinblighe/EnhancedVolcano. 2020.
81. http://bioinformaticspsbugentbe/webtools/Venn/.
82. Kolde R. pheatmap: Pretty Heatmaps. R package version 1012 https://CRANR-projectorg/package=pheatmap. 2019.
83. Ge SX, Jung D, Yao R. ShinyGO: a graphical gene-set enrichment tool for animals and plants. *Bioinformatics*. 2020;36:2628–2629. doi: 10.1093/bioinformatics/btz931